Frontiers in Bioscience Landmark

Front. Biosci. (Landmark Ed) **2026**; 31(6): 49296
https://doi.org/10.31083/FBL49296

Original Research

FGFR2 Regulates Liver Injury and Repair in a Model of Obstructive Jaundice

Weiwei Chu[1,†], Jinshan Liu[2,†], Jinlong Hu[2], Hongyu Xu[3], Xuanxuan Li[1], Peilin Liu[4], Dongquan Liu[2], Gan Chen[2], Baoqiang Cao[2], Jiaming Yao[1,2,*]

[1]Graduate School, Bengbu Medical University, 233000 Bengbu, Anhui, China
[2]Department of General Surgery, The First Affiliated Hospital of Anhui University of Chinese Medicine, 230031 Hefei, Anhui, China
[3]Graduate School, Anhui Medical University, 230041 Hefei, Anhui, China
[4]Graduate School, Anhui University of Science & Technology, 232001 Huainan, Anhui, China
*Correspondence: yjm_yao@163.com (Jiaming Yao)
[†]These authors contributed equally.
Academic Editor: Vesna Jacevic
Submitted: 20 December 2025 Revised: 1 May 2026 Accepted: 12 May 2026 Published: 24 June 2026

Abstract

Background: The molecular mechanisms underlying obstructive jaundice (OJ)-induced liver injury and subsequent repair after biliary recanalization (R-OJ) remain incompletely elucidated. This study aimed to identify and validate core gene involved in regulating OJ-related liver injury and repair via integrated *in vitro* and *in vivo* models. **Methods**: Animal models (OJ and R-OJ groups) and cell models (OJ serum (OJS) and OJ serum depletion (OJSD) groups) were established. Liver function and histopathologic changes were evaluated. Differentially expressed genes (DEGs) were screened by RNA sequencing (RNA-seq), and candidate genes were selected by intersecting DEGs with functional gene sets associated with "injury" and "repair". Key genes were identified via protein-protein interaction (PPI) network and pathway enrichment analyses. Fibroblast growth factor receptor 2 (FGFR2) expression was validated by quantitative reverse transcription PCR (qRT-PCR), Western blot, and immunohistochemistry (IHC). Functional involvement of FGFR2 was assessed by siRNA-mediated knockdown followed by assessment of downstream AKT signaling, proliferation (proliferating cell nuclear antigen, PCNA), and apoptosis maker cleaved caspase-3. **Results**: OJ induced significant liver dysfunction and tissue damage, which partially recovered after R-OJ. Bioinformatic analyses identified FGFR2 as a core regulatory gene among 20 candidates. FGFR2 was downregulated during injury (OJS vs. Con, $p < 0.05$) and upregulated during repair (OJSD vs. OJS, $p < 0.05$) both *in vivo* and *in vitro*. FGFR2 knockdown in BRL-3A cells markedly reduced p-AKT levels by approximately 50% under all serum conditions ($p < 0.01$), significantly decreased PCNA expression, and altered cleaved caspase-3 levels, suggesting that FGFR2 may contribute to hepatocyte proliferation and survival, potentially through the phosphoinositide 3-kinase (PI3K)/AKT signaling. **Conclusion**: FGFR2 exhibits a dynamic expression pattern of downregulation during cholestatic injury and upregulation during repair, and is associated with hepatocyte proliferation and apoptosis, potentially through AKT signaling. These findings suggest that FGFR2 may represent a potential therapeutic target for improving liver repair in obstructive jaundice.

Keywords: cholestasis; fibroblast growth factor receptor type 2; hepatocytes; jaundice, obstructive; liver regeneration; signal transduction

1. Introduction

Obstructive jaundice (OJ) is a common hepatobiliary disease caused by impaired bile excretion due to multiple factors, including intrahepatic bile duct stenosis, extrahepatic biliary stones, and tumor compression. Its core pathological feature is serum bilirubin accumulation and hepatocellular injury mediated by cholestasis [1]. Recent epidemiological studies have yielded updated assessments of the worldwide burden linked to OJ. A multicenter study carried out in Yemen, encompassing 303 patients, revealed an average age of 57 ± 17.99 years, with females constituting the majority (60.4% compared to 39.6% males). The primary causes identified included choledocholithiasis (57.8%), benign biliary strictures (19.1%), pancreatic head carcinoma (11.6%), and cholangiocarcinoma (6.9%) [2]. In a cohort from sub-Saharan Africa, OJ accounted for 0.6% of surgical admissions and 3% of hospitalizations due to non-traumatic abdominal conditions, with an in-hospital mortality rate as high as 18.2% [3]. Additionally, a Korean study involving 439 patients with severe hyperbilirubinemia (total bilirubin ≥12 mg/dL) reported 30-day mortality rates of 17.6% for benign hepatopancreatobiliary disorders, 42.9% for cirrhosis/malignancy, and 76.9% for ischemic injury. Notably, obstructive jaundice was identified as an independent predictor of 30-day mortality (hazard ratio = 2.42). Importantly, patients who underwent successful biliary decompression had a significantly lower mortality rate (15.0%) compared to those without mechanical obstruction (58.5%) [4]. Collectively, these findings highlight the substantial disease burden imposed by OJ and underscore the urgent

need for prompt therapeutic intervention. As the central organ for bile metabolism and excretion, the liver is prone to multiple pathophysiological disorders in the cholestatic microenvironment, mainly manifested as hepatic lobule destruction, hepatocellular apoptosis, inflammatory cell infiltration, and hepatic fibrosis [5]. Although drainage, the most commonly used clinical method for relieving biliary obstruction, effectively resolves the condition in most patients, some individuals still develop irreversible liver dysfunction following the procedure. The efficiency of liver repair following the relief of biliary obstruction is a critical determinant of patient prognosis, as a subset of patients may develop refractory hepatic fibrosis or even progress to liver failure due to delayed or impaired regenerative processes [6]. Therefore, systematically deciphering the molecular regulatory network of OJ-induced liver injury and repair, and identifying key regulatory targets, is of great theoretical and practical significance for optimizing clinical therapeutic strategies.

The pathological mechanism of OJ-related liver injury and repair is complex, involving cross-regulation of multiple pathways such as oxidative stress, inflammatory response, mitochondrial dysfunction, and cell apoptosis [7,8,9]. Previous studies have mostly relied on common bile duct ligation (CBDL) in rats to establish OJ models, focusing on gene expression changes at a single injury stage or simulating pathological processes through *in vitro* static cell models [10]. Acar et al. [11] demonstrated that administration of Turkey Rose oil via sublingual delivery over seven consecutive days in rats with bile duct ligation significantly reduced key indicators of acute liver injury associated with OJ, including elevated biochemical markers, portal inflammation, bile duct hyperplasia, polymorphonuclear leukocyte infiltration, and hepatic necrosis, thereby exerting a protective effect on liver tissue . However, the hepatic effects following the subsidence of obstruction have not been further clarified. Ozozan et al. [12] found that after biliary obstruction relief in OJ rats, hepatic mitochondrial number increased accompanied by lipid metabolism remodeling, suggesting the initiation of liver regeneration. However, the core molecules regulating this dynamic process remained unclear. Another study identified OJ-related differentially expressed genes (DEGs) via tissue RNA sequencing (RNA-seq), suggested that next generation sequencing can serve as a powerful tool to identify key molecular players involved in the progression of OJ and biliary recanalization (R-OJ) [13]. Ramachandran et al. [14] demonstrated through tissue RNA-seq that Matrix metalloproteinase 7 (MMP7) expression was significantly elevated in patients with persistent jaundice following Kasai portoenterostomy as well as in those with end-stage liver disease. In patients who achieved successful outcomes after Kasai portoenterostomy, Phosphoenolpyruvate carboxykinase 1 (PCK1) expression was upregulated, whereas it was markedly downregulated in patients with failed procedures, indicating outcome-specific expression patterns of MMP7 and PCK1 in biliary atresia [14]. However, tissue samples contain multiple cell types, making it difficult to accurately attribute hepatocyte-specific transcriptional regulation. In addition, tumor necrosis factor (TNF) induction is known to be one of the earliest events in hepatic inflammation, triggering a cascade of other cytokines that cooperate to kill hepatocytes, recruit inflammatory cells, and initiate a wound healing response that includes fibrogenesis [15]. Diehl found that, by comparing the hepatic response to TNF under conditions of liver injury promotion versus liver regeneration stimulation, TNF not only induces inflammatory reactions leading to hepatotoxicity but also triggers mitochondrial reactive oxygen species production, activates the nuclear factor-κB and Jun N-terminal kinase signaling pathways, upregulates various mitochondrial proteins, cytokine-inducible nitric oxide synthase, uncoupling protein-2, and other anti-apoptotic and antioxidant survival factors. These effects collectively inhibit apoptosis, reduce oxidative stress, and provide critical support for liver regeneration [16]. However, in existing research, the dual-role mediators involved in both injury and repair processes in models of OJ have not yet been fully explored. Therefore, an *in vitro* model for RNA-seq to simulate hepatocyte injury during OJ and recovery after relief of jaundice is necessary. Currently, no similar methods have been reported in the literature.

Fibroblast growth factor receptor 2 (FGFR2) plays critical roles in liver pathophysiology. Previous studies have established that FGFR2 signaling is essential for hepatocyte proliferation and liver regeneration. Padrissa-Altés et al. [17] demonstrated that expression of a dominant-negative FGFR2 mutant in hepatocytes impairs hepatocyte proliferation after partial hepatectomy, and combined loss of FGFR1, FGFR2, and FGFR4 in hepatocytes causes liver failure, revealing that FGFR signaling is indispensable for liver regeneration. In the context of liver fibrosis, FGFR2 has been implicated in the activation of hepatic stellate cells and the promotion of collagen deposition, and pharmacological inhibition of FGFR2 attenuates fibrogenesis in preclinical models [18]. The role of FGF/FGFR signaling in hepatic fibrosis has been comprehensively reviewed, highlighting FGFRs as promising therapeutic targets [19]. Epigenetic studies have further revealed that FGFR2 expression is upregulated in advanced liver fibrosis, with hypomethylation of its genomic region observed in patients with progressive NAFLD [20]. Mechanistically, activation of FGFR2b by its specific ligand FGF7 promotes hepatocyte survival and proliferation via AKT/ERK signaling, and ameliorates liver inflammation and fibrogenesis through paracrine mechanisms [21]. Additionally, FGFR2 has been identified as a key pro-fibrotic mediator through miRNA-dependent regulation in other fibrotic conditions, suggesting similar mechanisms may exist in hepatic fibrogenesis [22]. However, despite the established functions in regen-

eration and fibrosis, the dynamic expression and role of FGFR2 throughout the continuum of cholestatic liver injury and the repair process induced by biliary decompression, as observed in obstructive jaundice, remain largely unexplored.

In this study, we established animal and cell models and integrated RNA-seq with bioinformatics analysis to identify molecules that play a dual regulatory role during hepatocyte injury and repair in the OJ model, and further validated the expression pattern of related molecules.

2. Methods

2.1 Animals and Surgery

Thirty male Sprague-Dawley (SD) rats, aged 5 weeks and weighing 120 g, were purchased from Skbes Biotechnology Co., Ltd. (Henan, China). All rats were housed in a temperature-controlled environment (25 ± 2 °C), with five animals per cage, and had free access to standard chow and drinking water under a 12-hour light/12-hour dark cycle. Rats were acclimatized for one week prior to experimentation to adapt to laboratory conditions.

Successful establishment of the obstructive jaundice model was confirmed by the presence of visible jaundice (yellow discoloration of the skin, ears, and urine) and a serum total bilirubin level at least three times that of the Sham group at the time of sacrifice. Animals were excluded if they exhibited surgical complications (e.g., bile leakage, wound dehiscence, or infection) or if serum total bilirubin failed to reach the predefined threshold. Animals were monitored daily for signs of distress. Pre-defined humane endpoints included: body weight loss exceeding 20% compared to pre-surgery baseline; severe jaundice with marked lethargy; inability to eat or drink; wound dehiscence or infection; and any moribund condition. Animals reaching any humane endpoint would be immediately euthanized by deep isoflurane anesthesia followed by cervical dislocation and excluded from the study. In the present study, all 30 rats met the criteria for successful model establishment, no animals died or reached humane endpoints, and no data were excluded from analysis.

One week later, rats were randomly assigned to three groups using a random number table: the sham-operated (Sham) group, the OJ group, and the R-OJ group. For the Sham group, laparotomy was performed to expose the common bile duct without ligation. For the OJ group, after adequate exposure of the common bile duct, double ligation was performed with 4-0 silk sutures near the junction of the common bile duct and intestine. The initial surgical procedure for the R-OJ group was identical to that of the OJ group. One week after obstruction induction, a second laparotomy was performed to transect the ligated bile duct segment. Subsequently, end-to-side anastomosis was performed between the transected bile duct and intestinal opening using 4-0 silk sutures, and a silicone tube was placed in the anastomotic stoma as a stent to achieve R-OJ [23].

All rats were fasted and deprived of water for 12 h preoperatively. Anesthesia was induced with 3% isoflurane (Shandong Ante Animal Health Technology Co., Ltd., Shandong, China), and maintained with 1.5%–2.5% isoflurane throughout the surgery. Postoperatively, rats were allowed to recover under warm lighting for 30 minutes. At the end of the experimental period, rats were deeply anesthetized with 3% isoflurane and immediately euthanized by cervical dislocation. Complete cessation of respiration and heartbeat was confirmed before tissue and blood sample collection. Rats in the Sham and OJ groups were euthanized one week after the initial surgery, while those in the R-OJ group were euthanized one week after the second surgery. Blood and liver tissue samples were collected and stored at –80 ℃ for subsequent experiments. This study was approved by the Institutional Animal Care and Use Committee (IACUC) of our institution, and all animal procedures were conducted in compliance with the GB/T 35892-2018 Guidelines for the Ethical Review of Laboratory Animal Welfare (National Standard of the People's Republic of China). The study was carried out in accordance with the ARRIVE guidelines (Animal Research: Reporting of In Vivo Experiments).

2.2 Liver Function Test

Rat blood was collected and centrifuged at 3000 rpm for 10 minutes at 20 °C to separate serum. Serum levels of alanine aminotransferase (ALT), aspartate aminotransferase (AST), total bilirubin (TBIL), and direct bilirubin (DBIL) were measured using an automatic clinical analyzer (Chemray 800, Guangdong, China) [24].

2.3 Hematoxylin-Eosin (H&E) Staining

Liver tissues were fixed in 4% formaldehyde solution, embedded in paraffin, and sectioned into 5-μm-thick slices. H&E staining was performed to evaluate histopathological changes, and histological features were observed and documented under a light microscope [25].

2.4 Cell Culture

BRL-3A rat hepatocytes were purchased from Wuhan Pusai Life Science and Technology Co., Ltd. Cells were cultured in Minimum Essential Medium (MEM, Gibco, Waltham, MA, USA) supplemented with 10% fetal bovine serum (FBS, Gibco, USA) and 1% penicillin-streptomycin solution (Beyotime Biotechnology, Shanghai, China), and maintained in a humidified incubator with 5% CO_2 at 37 ℃. The culture medium was refreshed every 48 h.

Blood samples were collected from OJ model rats (n = 10) via cardiac puncture one week after the initial surgery. The blood was allowed to clot at room temperature for 30 min, followed by centrifugation at 3000 rpm for 15 min at 4 °C to collect the supernatant serum. Serum from all 10 rats were pooled to minimize individual variation. The pooled serum was heat-inactivated at 56 °C for 30 min to elimi-

nate complement activity and then sterilized by filtration through a 0.22 μm membrane filter. Aliquots were stored at –80 °C until further use. The use of disease serum in cell culture is a well-established approach to recapitulate the pathological microenvironment *in vitro*. Woolbright et al. [26] measured bile acid concentrations in serum from obstructive cholestasis patients and used these pathophysiological concentrations to treat primary human hepatocytes. Shen et al. [27] successfully used OJ rat serum to induce cholestatic liver injury in hepatocytes. Trovato et al. [28] further demonstrated that serum from liver failure patients directly modulates immune cell function. Thus, using OJ serum allows investigation of hepatocyte-specific responses to the cholestatic milieu while avoiding confounding effects from non-parenchymal cells.

BRL-3A cells were randomly divided into three groups: the control (Con) group, the OJ serum (OJS) group, and the OJ serum depletion (OJSD) group. Cells in the Con group were cultured in complete MEM containing 10% FBS and 1% penicillin-streptomycin. Cells in the OJS group were cultured in MEM supplemented with 10% serum from OJ rats and 1% penicillin-streptomycin. Cells in the OJS and Con groups were harvested after 24 h of culture. For the OJSD group, cells were cultured under the same conditions as the OJS group for the first 24 h, followed by culture in the Con group medium for an additional 24 h before harvesting. Collected cells were used for RNA-seq, Western blot, and Quantitative Reverse Transcription PCR (qRT-PCR) analyses.

The BRL-3A cell line underwent authentication through species-specific PCR targeting the mitochondrial *COI* gene, which verified its rat origin and the absence of cross-species contamination. Throughout the study, the cells were regularly tested for mycoplasma using a PCR-based approach and consistently yielded negative results.

2.5 Cell Cycle Analysis

BRL-3A cells from the Con, OJS, and OJSD groups were harvested by trypsinization, washed twice with ice-cold phosphate-buffered saline (PBS), and fixed in 70% ethanol overnight at 4 °C. After fixation, cells were centrifuged at 1000 rpm for 5 min and resuspended in PBS containing 50 μg/mL propidium iodide (PI) and 100 μg/mL RNase A (Servicebio Technology, Wuhan, Hubei, China). The suspension was incubated at 37 °C for 30 min in the dark.DNA content was acquired on a flow cytometer (Agilent Technologies, Santa Clara, CA, USA). A minimum of 10,000 events was recorded per sample. The gating strategy was performed as follows: (1) an initial gate was set on a forward scatter (FSC-A) versus side scatter (SSC-A) dot plot to exclude debris and select the intact cell population; (2) within the intact cell gate, doublets and aggregates were excluded using a pulse geometry gate (PI-A vs PI-W dot plot), retaining only singlet events for DNA content analysis; (3) the singlet population was displayed on a PI-A histogram, and the proportions of cells in G0/G1, S, and G2/M phases were fitted using the Watson pragmatic model in ModFit LT software (Verity Software House, Topsham, ME, USA). Data from three independent biological replicates were used for statistical analysis, and representative histograms from a single experiment are shown in Fig. 6A–C.

2.6 siRNA Transfection

BRL-3A cells were inoculated into 6-well plates at a density of 2×10^5 cells per well and cultured overnight until they attained 70–80% confluence. To suppress FGFR2 expression, the cells were transfected with 50 nM of FGFR2-specific siRNA (siFGFR2) or a scrambled negative control siRNA (siNC) using Lipofectamine™ 3000 reagent (ThermoFisher, USA) in accordance with the manufacturer's instructions [29]. The siRNA sequences used were as follows: siFGFR2: sense 5'-GCCAGGGAUAUCAACAACAUATT-3', antisense 5'-UAUGUUGUUGAUAUCCCUGGCTT-3', synthesized by GeneBio Co., Ltd. (Shanghai, China). siNC: sense 5'-UUCUCCGAACGUGUCACGUdTdT-3', antisense 5'-ACGUGACACGUUCGGAGAAdTdT-3', a scrambled non-targeting negative control siRNA, synthesized by GeneBio Co., Ltd. (Shanghai, China). Briefly, siRNA and Lipofectamine™ 3000 were separately diluted in serum-free MEM, gently mixed, and incubated at room temperature for 15 min to facilitate complex formation. Subsequently, the transfection complexes were added dropwise to the cells. After 6 h of incubation, the medium was replaced with fresh complete MEM, and the cells were allowed to grow for an additional 48 h. The knockdown efficiency was validated by qRT-PCR and Western blotting. After confirming the knockdown, the transfected cells were exposed to the specified serum conditions: the Con group was cultured in complete MEM supplemented with 10% FBS; the OJS group was cultured in MEM supplemented with 10% OJ serum; and the OJSD group was cultured in MEM containing 10% OJ serum for the initial 24 h, followed by a switch to MEM containing 10% FBS for the subsequent 24 h. After the serum treatment, Western blot analysis was performed as described in Section 2.9 to evaluate the expression of FGFR2 (knockdown efficiency), as well as AKT phosphorylation (p-AKT), total AKT, PCNA (proliferating cell nuclear antigen), and cleaved caspase-3.

2.7 RNA Isolation and RNA-Seq

Total RNA was isolated from cells of each experimental group using TRIzol® reagent (Invitrogen, Thermo Fisher Scientific, Suzhou, China). RNA integrity and purity were verified by ensuring an A260/A280 ratio between 1.8 and 2.0. Polyadenylated mRNA was captured from the total RNA pool with Oligo(dT)-conjugated magnetic beads (Beyotime Biotechnology, Shanghai, China) and subsequently fragmented into segments of approxi-

mately 150–200 nucleotides. First-strand cDNA was synthesized from the fragmented mRNA using SuperScript™ II reverse transcriptase (Thermo Fisher Scientific, Suzhou, China), followed by second-strand synthesis employing RNase H and DNA polymerase I (Thermo Fisher Scientific, Shanghai, China) with random primers. The resulting double-stranded cDNA underwent end-repair, 3′ adenylation, and adapter ligation prior to PCR enrichment to generate the final cDNA library. Library quality was assessed on an Agilent 2100 Bioanalyzer before sequencing on an Illumina platform. Raw sequencing data were stored in FASTQ format, and quality control was performed concurrently. High-quality clean reads were obtained by filtering the raw sequences with Cutadapt software (National Bioinformatics Infrastructure Sweden, Sweden, https://cutadapt.readthedocs.io/). These clean reads were then aligned to the rat reference genome (rno) using HISAT2. Reads uniquely mapped to annotated genomic or exonic regions were enumerated, and transcript abundance was quantified with StringTie software (Center for Computational Biology, Johns Hopkins University, Baltimore, MD, USA) [30].

2.8 Analysis of RNA-Seq Results

To identify DEGs among the Con, OJS, and OJSD groups (including known and unknown genes in annotation files), differential gene analysis was performed using DESeq2 software (a widely used tool for DEG analysis with biological replicates, Bioconductor, USA, https://bioconductor.org/packages/release/bioc/html/DESeq2.html). A gene was defined as a statistically significant DEG if the adjusted p-value < 0.05 and $|\log_2(\text{fold change})| > 1$. Subsequently, Gene Ontology (GO) and Kyoto Encyclopedia of Genes and Genomes (KEGG) annotations were performed to explore potential regulatory pathways, and enrichment analysis was conducted using the clusterProfiler package in R ($p < 0.05$ as the cutoff for significant enrichment). “Injury” and “repair” gene sets (top 10% protein-coding genes) were retrieved from the GeneCards database(https://www.genecards.org/) [31] by inputting the corresponding keywords. Results were visualized as Venn diagrams, heatmaps and volcano using the VennDiagram, pheatmap and ggplot2 R packages respectively. Protein-protein interaction (PPI) network was constructed using the STRING database and visualized with Cytoscape 3.9.0 software (Cytoscape Consortium, San Diego, CA, USA).

2.9 Quantitative Reverse Transcription PCR (qRT-PCR)

Total RNA was extracted from cells using TRIzol® reagent (Absin, Shanghai, China) and reverse-transcribed into cDNA with the TransGen Reverse Transcription Kit (TransGen Biotech Co., Ltd., Beijing, China). qRT-PCR was performed on a LightCycler® 96 Real-Time PCR System (Roche Diagnostics, Switzerland) using SYBR Green I reagent. Glyceraldehyde-3-phosphate dehydrogenase (GAPDH) was used as the internal reference gene, and relative gene expression levels were calculated using the $2^{-\Delta\Delta CT}$ method [32] (Table 1).

2.10 Western Blot

BRL-3A cells from each group were harvested and lysed with RIPA lysis buffer (Servicebio, China) on ice for 30 min. Lysates were centrifuged at 12,000 rpm for 10 min at 4 °C, and the supernatant was collected as total protein extract. Protein concentration was quantified using a BCA Protein Assay Kit (Servicebio, China). Protein samples were separated by 10% SDS-PAGE (Servicebio, China) and transferred onto polyvinylidene fluoride (PVDF) membranes (Servicebio, China). Membranes were blocked with 5% non-fat dry milk in TBST at room temperature for 1 h, followed by overnight incubation with primary antibodies at 4 °C. After washing three times with TBST (5 min per wash), membranes were incubated with corresponding secondary antibodies at room temperature for 30 min. Immunocomplexes were visualized using Tanon™ Femto Sig ECL chemiluminescent substrate (Servicebio, China), and signals were detected using a chemiluminescence imaging system [33]. Antibodies used: anti-FGFR2 antibody (MA5-32629, 1:1000 dilution, Thermo Fisher Scientific, China), anti-GAPDH antibody (GB15004, 1:5000 dilution, Servicebio Biotechnology Co., Ltd., China), anti-p-AKT antibody (9271T, 1:1000 dilution, Cell Signaling Technology, Inc., USA), anti-AKT antibody (4691T, 1:1000 dilution, Cell Signaling Technology, Inc., USA), anti-PCNA antibody (13110T, 1:1000 dilution, Cell Signaling Technology, Inc., USA), anti-Cleaved caspase3 antibody (14220T, 1:1000 dilution, Cell Signaling Technology, Inc., USA), anti-p-STAT3 antibody (9145T, 1:2000 dilution, Cell Signaling Technology, Inc., USA), anti-STAT3 antibody (12640T, 1:1000 dilution, Cell Signaling Technology, Inc., USA), anti-p-ERK1/2 antibody (4370T, 1:2000 dilution, Cell Signaling Technology, Inc., USA), anti-ERK1/2 antibody (4695T, 1:1000 dilution, Cell Signaling Technology, Inc., USA).

2.11 Immunohistochemistry (IHC)

Paraffin-embedded liver sections were first dewaxed by passage through a graded series of xylene and ethanol solutions, followed by rehydration to water. Heat-induced antigen retrieval was subsequently performed to unmask epitopes. Following a wash with phosphate-buffered saline (PBS), endogenous peroxidase activity was quenched by incubation with 3% hydrogen peroxide, and non-specific protein binding was minimized by blocking with 3% bovine serum albumin (BSA) for 30 min. Tissue sections were then probed overnight at 4 °C with an anti-FGFR2 primary antibody (1:100 dilution; Thermo Fisher Scientific, China). After three successive washes with PBS, sections were incubated with an HRP-conjugated goat anti-rabbit secondary antibody (1:500 dilution; Servicebio, China) for 50 min at

Table 1. Primer sequences used for quantitative real-time PCR (qRT-PCR).

Gene	Primer sequence (5′→3′)	Product size (bp)	Annealing temp (°C)	Cycle	Source
FGFR2	F:CCCACTGGTGAGGATAACGAC	166	60	40	Designed in this study based on
	R: CATGACTACTTGCCCGAAGC				GenBank NM_001109892.1
GAPDH	F: CTGGAGAAACCTGCCAAGTATG	138	60	40	Designed in this study based on
	R: GGTGGAAGAATGGGAGTTGCT				GenBank NM_017008.4

FGFR2, fibroblast growth factor receptor 2; GAPDH, Glyceraldehyde-3-phosphate dehydrogenase.

room temperature. Immunoreactivity was visualized using 3,3′-diaminobenzidine (DAB) as the chromogen, with the reaction duration monitored microscopically to achieve optimal signal intensity. Nuclei were counterstained with hematoxylin. Finally, the stained sections were dehydrated through an ascending ethanol series, cleared in xylene, and mounted with coverslips. Images were acquired and evaluated under a light microscope [34].

2.12 Statistical Analysis

Statistical analyses were conducted using Prism 9.5.0 (GraphPad Software, San Diego, CA, USA) and SPSS 27.0 software (IBM Corporation, Armonk, NY, USA). Continuous variables conforming to a normal distribution are presented as $X \pm s$, while those not conforming to a normal distribution are expressed as M (P25, P75). For comparisons of continuous variables between groups, the Mann-Whitney U test or *t*-test was employed. A two-tailed test was applied for statistical results, with a significance level set at $p < 0.05$. For the analysis of DEGs, log2 transformation of counts (logCPM) was initially performed, followed by analysis using the "limma" software package. The empirical Bayesian method was utilized to adjust gene expression levels, thereby enhancing the accuracy of DEG detection. The false discovery rate (FDR) control method was applied for multiple comparison test correction, with a significance level of $p < 0.05$. For other data conforming to a normal distribution, an unpaired *t*-test was used to analyze differences between groups, with the significance level also set at $p < 0.05$. All data are presented as mean ± SD from biological replicates.

3. Results

3.1 Liver Function Change Induced by Biliary Obstruction and Recanalization

To evaluate the dynamic change of biliary obstruction and recanalization on liver function, serum levels of TBIL, DBIL, ALT, and AST were measured. As shown in Table 2, compared with the Sham group, these liver function parameters were significantly elevated in the OJ group ($p < 0.05$). Compared with the OJ group, these liver function parameters were significantly declined in the R-OJ group ($p < 0.05$). The results indicated that OJ leads to hepatic dysfunction, and partial recovery of liver function occurs during R-OJ.

3.2 Liver Tissue Structure Change Induced by Biliary Obstruction and Recanalization

To further investigate whether liver tissue architecture undergoes changes analogous to those observed in the serum liver function tests described above. H&E staining was performed to characterize histopathological changes in liver tissue. As shown in Fig. 1A,B, no abnormal hepatic structure was observed in the Sham group. As shown in Fig. 1C,D, in the OJ group, Liver tissues exhibited severe pathological alterations, including disruption of hepatic lobule architecture, loss of the radial arrangement of hepatocyte cords, marked narrowing of hepatic sinusoids, impaired anatomical continuity between central veins and portal tracts, significant expansion of portal areas into hepatic lobules, and formation of fibrous septa due to extensive fibrous tissue proliferation. Hepatocytes displayed severe structural damage, characterized by extensive steatosis and necrosis, enhanced cytoplasmic eosinophilia, and hyperchromatic nuclei with distinct outlines. These results suggested that OJ leads to liver tissue structure damage.

As shown in Fig. 1E,F, the R-OJ group exhibited significantly alleviated pathological damage at the tissue level compared to the OJ group, characterized by a tendency toward radial arrangement of hepatocyte cords with only mild local disorganization and marked reduction in portal area expansion and fibrous tissue proliferation. Additional pathological improvements at the cellular level were observed, including alleviation of hepatocyte swelling, more uniform cell size, substantial decrease in the number of cytoplasmic eosinophilic granules and necrotic hepatocytes, and the presence of only a few residual necrotic foci with diminished surrounding inflammatory cell infiltration. These results indicated that during R-OJ, the damaged liver tissue architecture was partially restored.

3.3 Identification of DEGs

To identify DEGs in an *in vitro* model simulating OJ and obstruction relief, RNA-seq and bioinformatics analyses were performed using BRL-3A hepatocytes derived from the Con, OJS, and OJSD groups (three biological replicates per group). As shown in **Supplementary Table 1**, each RNA-seq sample yielded an average of $(29.0 \pm 4.0) \times 10^6$ high-quality clean reads, with (80.71% ± 1.55%) uniquely mapped to the rat reference genome. Using the cutoff criteria of adjusted *p*-value < 0.05 and $|\log_2 FC| > 1$, as shown in **Supplementary Table 2** and Fig. 2A, 1997 DEGs

Table 2. Serum biochemical parameters of rats in Sham, OJ and R-OJ groups.

	ALT	AST	TBIL	DBIL
Sham	42.23 ± 6.62	111.75 ± 31.11	16.68 ± 3.81	10.25 ± 2.39
OJ	214.89 ± 51.11	738.92 ± 97.14	227.01 ± 55.59	158.77 ± 29.75
R-OJ	90.91 ± 17.97	279.74 ± 43.40	67.89 ± 16.01	65.93 ± 15.57
t1	–10.593	–19.444	–11.936	–15.737
t2	7.236	13.648	8.696	8.741
P1	0.000***	0.000***	0.000***	0.000***
P2	0.000***	0.000***	0.000***	0.000***

Data are presented as mean ± SD, n = 10 per group. ALT, alanine aminotransferase; AST, aspartate aminotransferase; TBIL, total bilirubin; DBIL, direct bilirubin; OJ, obstructive jaundice; R-OJ, biliary recanalization. Statistical significance is indicated as follows: ***, $p < 0.001$.

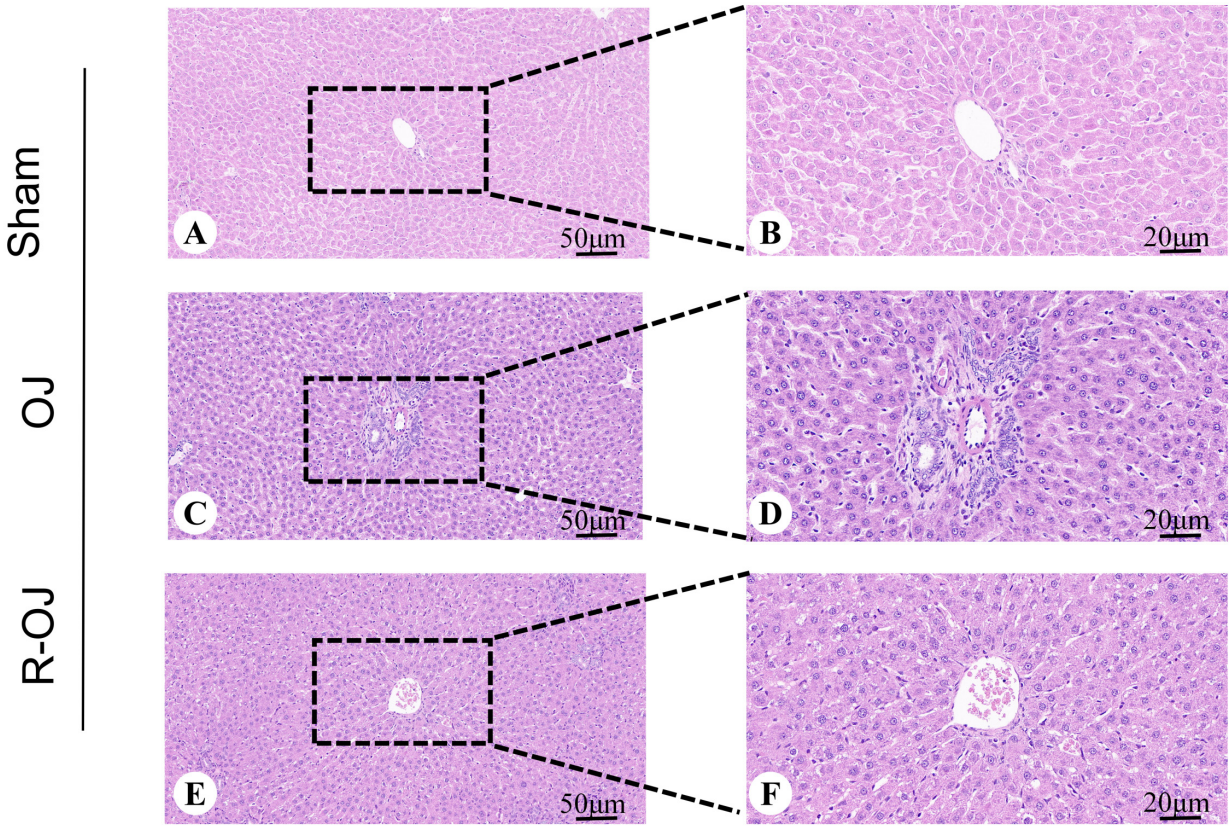

Fig. 1. Histopathological changes in rat liver tissues assessed by H&E staining. (A) Representative image of liver tissue from the Sham group showing normal hepatic lobule architecture and radial arrangement of hepatocyte cords (scale bar = 50 μm). (B) Higher magnification of (A) showing normal hepatocyte morphology with distinct nuclei and cytoplasm (scale bar = 20 μm). (C) Representative image of liver tissue from the OJ group showing severe disruption of hepatic lobule architecture, loss of radial arrangement, and marked fibrous tissue proliferation (scale bar = 50 μm). (D) Higher magnification of (C) showing extensive hepatocyte steatosis, necrosis, and inflammatory cell infiltration (scale bar = 20 μm). (E) Representative image of liver tissue from the R-OJ group showing partial restoration of hepatic architecture with reduced fibrosis (scale bar = 50 μm). (F) Higher magnification of (E) showing alleviated hepatocyte damage and decreased inflammatory infiltration (scale bar = 20 μm). H&E, Hematoxylin-Eosin.

were identified between the OJS and Con groups (1030 upregulated, 967 downregulated), designated as DEGs1. As shown in **Supplementary Table 3** and Fig. 2B, 1814 DEGs between the OJS and OJSD groups (699 upregulated, 1115 downregulated), designated as DEGs2. As shown in **Supplementary Table 4** and Fig. 2C, 979 genes were identified by intersecting DEGs1 and DEGs2 and were designated as DEGs3. These genes are presumed to be potentially in-

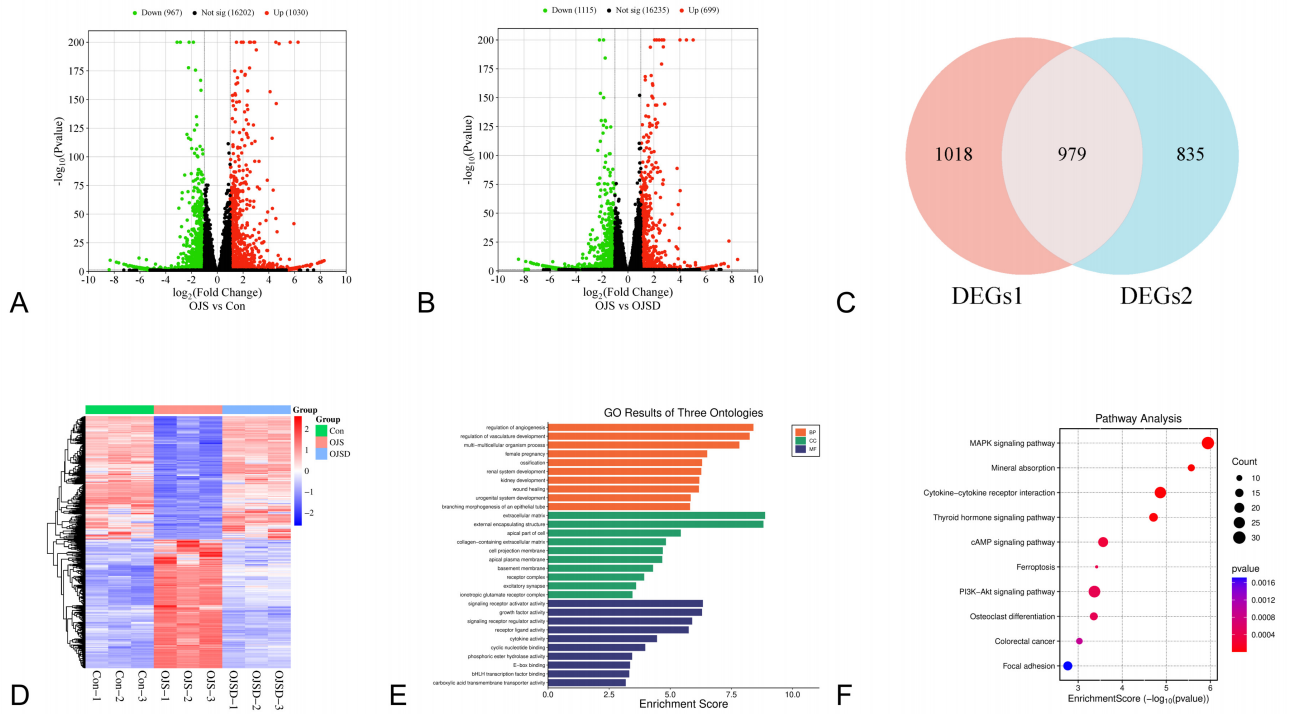

Fig. 2. Identification and enrichment analysis of differentially expressed genes in Con, OJS and OJSD groups. (A) Volcano plot showing DEGs between the OJS and Con groups. Red dots indicate significantly upregulated genes ($|\log_2 FC| > 1$, $p < 0.05$), green dots indicate significantly downregulated genes, and black dots indicate genes with no significant difference. (B) Volcano plot showing DEGs between the OJS and OJSD groups, with color coding as in (A). (C) Venn diagram showing the intersection of DEGs1 (OJS vs. Con) and DEGs2 (OJS vs. OJSD), identifying 979 co-expressed genes (DEGs3). (D) Heatmap showing the clustered expression profiles of DEGs3 across Con, OJS and OJSD groups. Each column represents a sample, each row represents a gene; red indicates high expression, blue indicates low expression. (E) GO enrichment analysis of DEGs3, showing the top 10 enriched terms in biological processes, cellular components, and molecular functions. (F) KEGG pathway enrichment analysis of DEGs3, showing the top 10 significantly enriched pathways. Con, control; OJS, OJ serum; OJSD, OJ serum depletion; DEGs, differentially expressed genes; GO, Gene Ontology; KEGG, Kyoto Encyclopedia of Genes.

volved in the overall biological regulation during OJ and R-OJ. As shown in Fig. 2D, heatmap analysis revealed the clustered expression profiles of DEGs across samples.

3.4 Functional Enrichment Analysis of DEGs

To further investigate the biological functions and potential signaling pathways associated with the DEGs in an *in vitro* model simulating OJ and obstruction relief described above, GO and KEGG analyses were performed. As shown in **Supplementary Table 5** and Fig. 2E, functional enrichment analysis was performed on DEGs3 to explore their biological functions. The results of GO enrichment analysis showed that multiple signaling pathways were potentially associated with tissue damage and repair, including regulation of angiogenesis (GO:0045765, BP, $p = 3.98 \times 10^{-9}$), Wound healing (GO:0042060, BP, $p = 6.73 \times 10^{-7}$), Extracellular matrix (GO:0031012, CC, $p = 1.33 \times 10^{-9}$), Basement membrane (GO:0005604, CC, $p = 5.05 \times 10^{-5}$), Growth factor activity (GO:0008083, MF, $p = 5.02 \times 10^{-7}$), etc. Similarly, as shown in **Supplementary Table 6** and Fig. 2F, functional enrichment analysis was performed on DEGs3 to explore their signaling pathways. The results of KEGG enrichment analysis showed that multiple signaling pathways were potentially associated with tissue damage and repair, including, MAPK signaling pathway (rno04010, $p = 1.14 \times 10^{-6}$), PI3K-Akt signaling pathway (rno04151, $p = 4.26 \times 10^{-4}$), Focal adhesion (rno04510, $p = 1.71 \times 10^{-3}$), ECM-receptor interaction (rno04512, $p = 2.00 \times 10^{-3}$), Chemical carcinogenesis-receptor activation (rno05207, $p = 2.00 \times 10^{-3}$), IL-17 signaling pathway (rno04657, $p = 2.17 \times 10^{-3}$), Efferocytosis (rno04148, $p = 3.20 \times 10^{-3}$), Calcium signaling pathway (rno04020, $p = 3.43 \times 10^{-3}$), TNF signaling pathway (rno04668, $p = 5.18 \times 10^{-3}$), etc. These results suggested that OJ and recanalization may be involved in the processes of tissue injury and repair through the aforementioned signaling pathways.

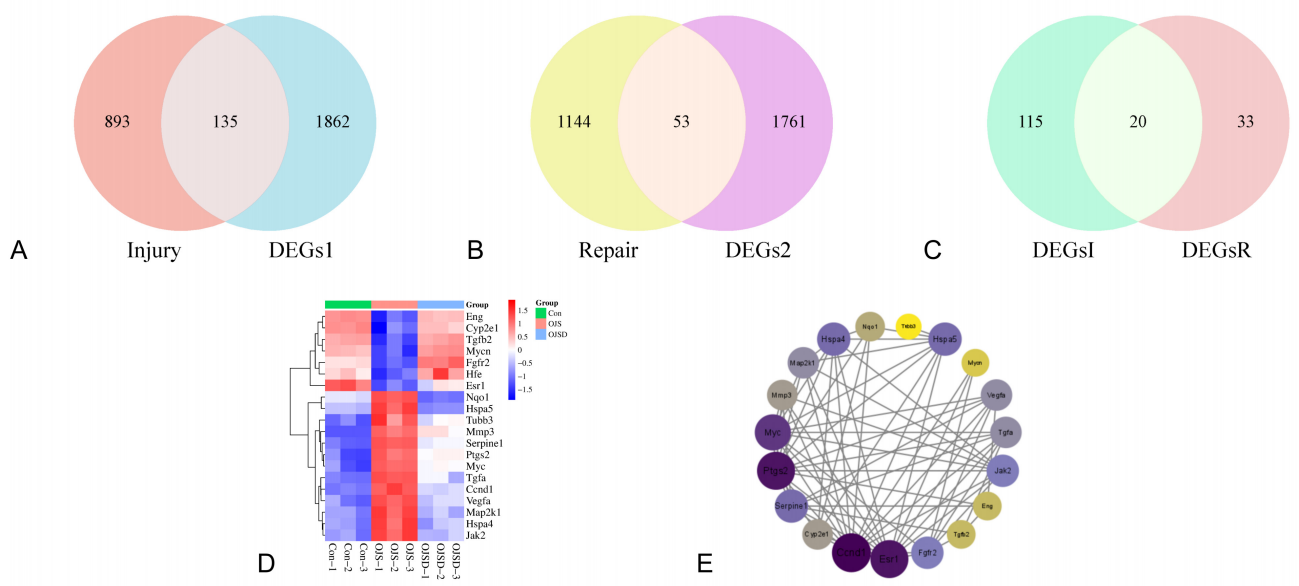

Fig. 3. Expression of injury and repair genes in an *in vitro* obstructive jaundice model. (A) Venn diagram showing the overlap between DEGs1 and the "injury" gene set from the GeneCards database, identifying 135 commonly regulated genes (DEGsI). (B) Venn diagram showing the overlap between DEGs2 and the "repair" gene set, identifying 53 commonly regulated genes (DEGsR). (C) Venn diagram showing the intersection of DEGsI and DEGsR, identifying 20 candidate genes, including SERPINE1, PTGS2, VEGFA, MAP2K1, ENG, HSPA4, CYP2E1, CCND1, MYC, FGFR2, MMP3, ESR1, TGFB2, JAK2, HSPA5, TUBB3, MYCN, HFE, TGFA, and NQO1. (D) Heatmap showing the expression patterns of the 20 candidate genes across Con, OJS and OJSD groups. (E) Protein-protein interaction (PPI) network of 19 candidate genes constructed using the STRING database and visualized with Cytoscape 3.9.0. Node size represents degree value (number of connections), edge thickness represents interaction confidence score.

3.5 Analysis of Injury-Repair-Related Genes in the OJ Model

To screen key genes involved in damage and repair using an *in vitro* model simulating OJ and obstruction relief, RNA-Seq data were intersected with the "injury" and "repair" gene sets in GeneCards database. As shown in **Supplementary Table 7** and Fig. 3A, 135 overlapping genes were identified between DEGs1 and the "injury" gene set, designated as DEGsI. As shown in **Supplementary Table 8** and Fig. 3B, 53 overlapping genes between DEGs2 and the "repair" gene set, designated as DEGsR. As shown in **Supplementary Table 9** and Fig. 3C, after DEGsI and DEGsR were intersected, 20 candidate genes were identified, including SERPINE1, PTGS2, VEGFA, MAP2K1, ENG, HSPA4, CYP2E1, CCND1, MYC, FGFR2, MMP3, ESR1, TGFB2, JAK2, HSPA5, TUBB3, MYCN, HFE, TGFA, and NQO1. As shown in Fig. 3D, The clustered expression profiles of the 20 candidate genes in each group were visualized by heatmap analysis. As shown in Fig. 3E, a PPI network of the 20 candidate genes was constructed using the STRING database and visualized with Cytoscape 3.9.0 software, resulting in 19 nodes used for network diagram construction.

As shown in **Supplementary Table 10**, after sorting by node degree, genes with a degree value of ≥8 were selected and integrated with the top three enriched pathways from the KEGG enrichment analysis of DEGs3. Subsequently, FGFR2 was identified as a key gene involved in regulating hepatic injury and repair processes in the OJ model.

3.6 Validation of FGFR2 Expression in OJ Model

To verify the expression of FGFR2 in the *in vivo* model, IHC was performed to detect its expression in rat liver tissue. As shown in Fig. 4, compared with the Sham group, the expression of FGFR2 was significantly down-regulated in the OJ group ($p < 0.05$). In contrast, compared with the OJ group, the expression of FGFR2 was significantly upregulated in the R-OJ group ($p < 0.05$). To verify the reliability of RNA-Seq results, the expression of FGFR2 was detected in the BRL-3A hepatocyte model *in vitro* using qRT-PCR and Western blot. As shown in Fig. 5A, compared with the Con group, the expression of FGFR2 mRNA in the OJS group was significantly decreased ($p < 0.05$), whereas in the OJSD group, it was significantly increased ($p < 0.05$) compared to the OJS group. Similarly, compared with the Con group, Western blot results showed that the protein expression of FGFR2 in the OJS group was significantly down-regulated ($p < 0.05$), while that in the OJSD group was up-regulated ($p < 0.05$) compared to the OJS group (Fig. 5B).

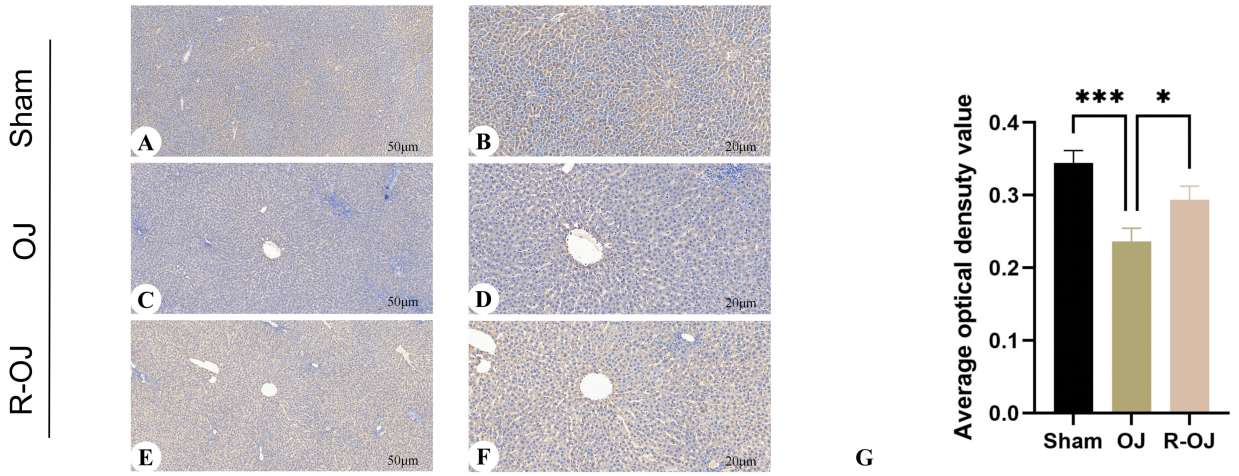

Fig. 4. Immunohistochemical detection of FGFR2 expression in rat liver tissues. (A) Positive expression of FGFR2 in liver tissues of the Sham group (scale bar = 50 μm). (B) Higher magnification of (A) showing FGFR2-positive signals mainly localized in the cell membrane of hepatocytes (scale bar = 20 μm). (C) Positive expression of FGFR2 in liver tissues of the OJ group (scale bar = 50 μm). (D) Higher magnification of (C) showing significantly weaker FGFR2 expression compared to the Sham group (scale bar = 20 μm). (E) Positive expression of FGFR2 in liver tissues of the R-OJ group (scale bar = 50 μm). (F) Higher magnification of (E) showing markedly recovered FGFR2 expression compared to the OJ group (scale bar = 20 μm). (G) Quantitative analysis of FGFR2 expression as average optical density (AOD) values. Data are presented as mean ± SD, n = 6. Statistical significance is indicated as follows: *, $p < 0.05$; ***, $p < 0.001$.

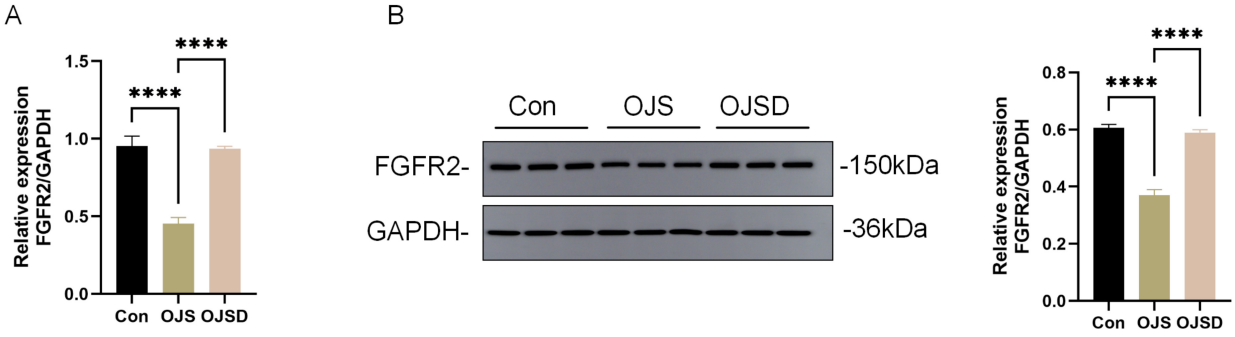

Fig. 5. Validation of FGFR2 expression in an *in vitro* obstructive jaundice model by qRT-PCR and Western blot. (A) qRT-PCR analysis of FGFR2 mRNA expression levels in BRL-3A cells from Con, OJS and OJSD groups. GAPDH was used as an internal reference. Data are presented as mean ± SD, n = 3. (B) Western blot analysis of FGFR2 protein expression levels in BRL-3A cells from Con, OJS and OJSD groups. GAPDH was used as a loading control. Left panel: representative immunoblot images. Right panel: densitometric quantification of FGFR2 protein levels normalized to GAPDH. Data are presented as mean ± SD, n = 3. Statistical significance is indicated as follows: ****, $p < 0.0001$. qRT-PCR, quantitative real-time polymerase chain reaction.

Collectively, these results demonstrated that FGFR2 exhibits a dynamic expression pattern of "downregulation during injury and upregulation during repair" in the OJ model.

3.7 OJ Serum Reversibly Decreases the Proportion of BRL-3A Cells in the S Phase

To determine whether cholestatic serum affects hepatocyte cell cycle progression, flow cytometric analysis was performed on BRL-3A cells cultured under Con, OJS, and OJSD conditions. As shown in Fig. 6, panels A, B, and C sequentially represent the typical cell cycle diagrams for the Con group, OJS group, and OJSD group, respectively. As shown in Fig. 6D, the proportion of cells in G1 phase was significantly increased in the OJS group (52.86% ± 0.08%) compared with the Con group (41.57% ± 0.09%; $p < 0.01$). Following the removal of OJ serum, the G2 fraction in the OJSD group decreased to 45.18% ± 0.17%, which was sig-

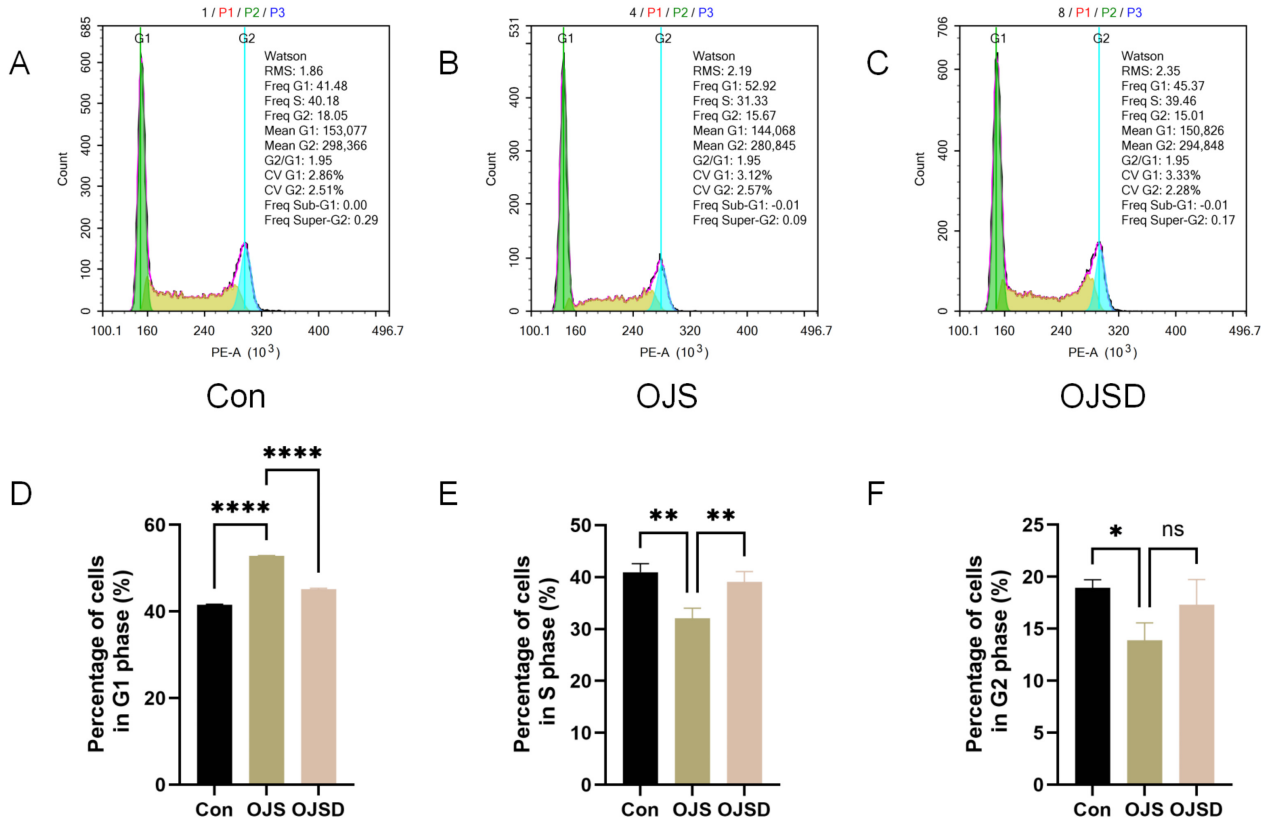

Fig. 6. Analysis of the cell cycle in BRL-3A cells cultivated under varying serum conditions. (A–C) Representative flow cytometry histograms depicting the distribution of DNA content in the Con, OJS, and OJSD groups from one experimental trial. (D) Quantitative assessment of the proportion of cells in the G1 phase. Data are expressed as mean ± SD from three independent experiments (n = 3). (E) Quantitative assessment of the proportion of cells in the S phase. Data are expressed as mean ± SD from three independent experiments (n = 3). (F) Quantitative assessment of the proportion of cells in the G2 phase. Data are expressed as mean ± SD from three independent experiments (n = 3). Statistical significance is indicated as follows: *, $p < 0.05$; **, $p < 0.01$; ****, $p < 0.0001$; ns, not significant.

nificantly lower than that in the OJS group ($p < 0.01$). As shown in Fig. 6E, the percentage of cells in S phase was significantly reduced in the OJS group (32.06% ± 1.91%) compared with the Con group (40.93% ± 1.70%; $p < 0.01$). Following the removal of OJ serum, the S phase fraction in the OJSD group recovered to 39.05% ± 2.02%, which was significantly higher than that in the OJS group ($p < 0.01$) and did not differ significantly from the Con group ($p > 0.05$). As shown in Fig. 6F, the percentage of cells in G2 phase was significantly decreased in the OJS group (13.91% ± 1.65%) compared with the Con group (18.94% ± 0.79%; $p < 0.05$). Following the removal of OJ serum, the G2 fraction in the OJSD group recovered to 17.30% ± 2.43%; however, this value was not significantly different from the OJS group ($p > 0.05$). These findings demonstrate that the cholestatic microenvironment induces a reversible attenuation of hepatocyte cell cycle progression, and that restoration of a physiological serum environment is sufficient to restore normal proliferative capacity.

3.8 Validation of FGFR2 Knockdown in BRL-3A Cells

To assess the knockdown efficacy of FGFR2-specific siRNA, BRL-3A cells were transfected with either siFGFR2, siFGFR2-1, siFGFR2-2 or siNC, followed by evaluation of FGFR2 expression at both the mRNA and protein levels. qRT-PCR analysis indicated that the relative mRNA expression of FGFR2 was most significantly decreased in the siFGFR2 group compared to the siNC group ($p < 0.05$; Fig. 7A). In line with the transcriptional repression, Western blot analysis revealed a significant reduction in FGFR2 protein levels in siFGFR2-transfected cells relative to the siNC control, with the difference being statistically significant ($p < 0.01$; Fig. 7B). Overall, these findings demonstrate that siFGFR2 transfection effectively inhibits FGFR2 expression in BRL-3A hepatocytes.

3.9 FGFR2 Knockdown Suppresses AKT Phosphorylation, Reduces PCNA Expression, and Increases Cleaved Caspase-3 Levels in BRL-3A Cells

To investigate the functional consequences of FGFR2 loss, we examined the protein levels of key downstream

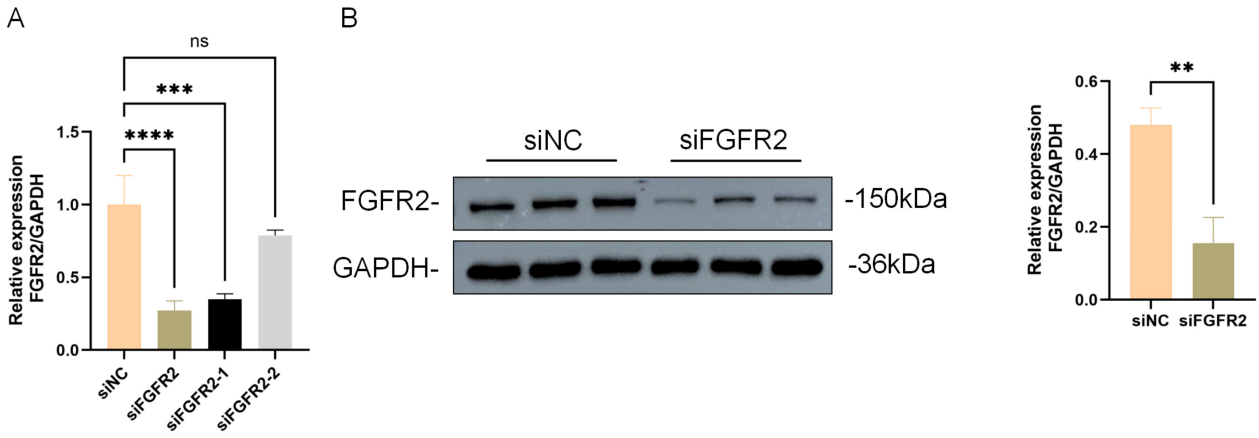

Fig. 7. Validation of FGFR2 knockdown efficiency in BRL-3A hepatocytes. (A) qRT-PCR analysis of FGFR2 mRNA levels. GAPDH was used as internal control. (B) Western blot analysis of FGFR2 protein expression; GAPDH as internal control. Data are mean ± SD (n = 3). Statistical significance is indicated as follows: **, $p < 0.01$; ***, $p < 0.001$; ****, $p < 0.0001$; ns, not significant. siNC, negative control siRNA; siFGFR2, FGFR2-specific siRNA.

molecules in siNC- and siFGFR2-transfected BRL-3A cells cultured under Con, OJS, and OJSD conditions.

AKT phosphorylation: As shown in Fig. 8A,B, total AKT protein levels remained unchanged across all groups, confirming equal protein loading. FGFR2 knockdown significantly reduced the p-AKT by approximately 50% in all three serum conditions compared with the corresponding siNC controls (all $p < 0.01$). Notably, the magnitude of reduction was similar across Con, OJS, and OJSD groups, indicating that FGFR2 contributes equally to AKT activation regardless of the serum microenvironment.

PCNA expression: The proliferation marker PCNA was significantly down-regulated in siFGFR2-transfected cells compared with siNC controls under all three conditions (Fig. 8C,D). In siNC cells, PCNA expression in the OJS group was reduced compared to the Con group ($p < 0.05$), while PCNA expression in the OJSD group showed significant recovery. In siFGFR2 cells, PCNA levels were further reduced, with the most pronounced decrease observed in the OJSD group (vs. siNC-OJSD, $p < 0.01$). Interestingly, within the siFGFR2 group, there was no statistically significant difference in PCNA expression between OJS and OJSD ($p > 0.05$), suggesting that FGFR2 knockdown abolished the repair-phase recovery of proliferation.

Cleaved caspase-3 expression: As shown in Fig. 8E,F, in siNC cells, cleaved caspase-3 levels were significantly elevated in the OJS group compared with Con ($p < 0.05$), indicating that cholestatic injury induced apoptosis. However, there was no statistically significant difference between OJS and OJSD ($p > 0.05$), suggesting that the 24-h repair period was insufficient to reverse the apoptotic program once activated. In siFGFR2-transfected cells, cleaved caspase-3 levels were generally higher than in siNC cells under all three conditions, consistent with a pro-apoptotic effect of FGFR2 loss. Notably, in the OJSD repair group, siFGFR2 cells exhibited significantly lower cleaved caspase-3 levels than siNC-OJSD cells ($p < 0.05$). This unexpected finding indicates that FGFR2 knockdown not only failed to resolve apoptosis during repair but paradoxically led to a reduction of cleaved caspase-3 below the level observed in control repair cells. The mechanistic basis for this observation remains to be determined but may reflect a shift in cell death modality (e.g., from apoptosis to other forms of regulated cell death) or a selection of a more resistant hepatocyte subpopulation in the absence of FGFR2.

Collectively, these results demonstrate that FGFR2 is a critical upstream activator of AKT, contributing approximately half of total p-AKT activity. FGFR2 knockdown uniformly reduces PCNA and increases cleaved caspase-3 across all conditions. However, the dynamics during repair reveal dissociated behaviors: while PCNA recovery in OJSD is completely dependent on FGFR2, the apoptotic response does not reverse within 24 h and is unexpectedly diminished upon FGFR2 loss in the repair phase. These findings highlight the complex and context-dependent role of FGFR2 in coordinating hepatocyte proliferation and survival.

3.10 Impact of FGFR2 Knockdown on the Phosphorylation of ERK and STAT3

To investigate whether FGFR2 modulates the MAPK/ERK and JAK-STAT signaling pathways, we assessed the phosphorylation status of ERK1/2 and STAT3 in BRL-3A cells transfected with siNC or siFGFR2, cultured under Con, OJS, and OJSD conditions. As depicted in Fig. 9, no notable differences in the levels of p-ERK or p-STAT3 were detected between the siNC and siFGFR2 groups across all three serum conditions (all $p > 0.05$, two-way ANOVA). Additionally, within each transfection group, the three serum conditions had no significant effect

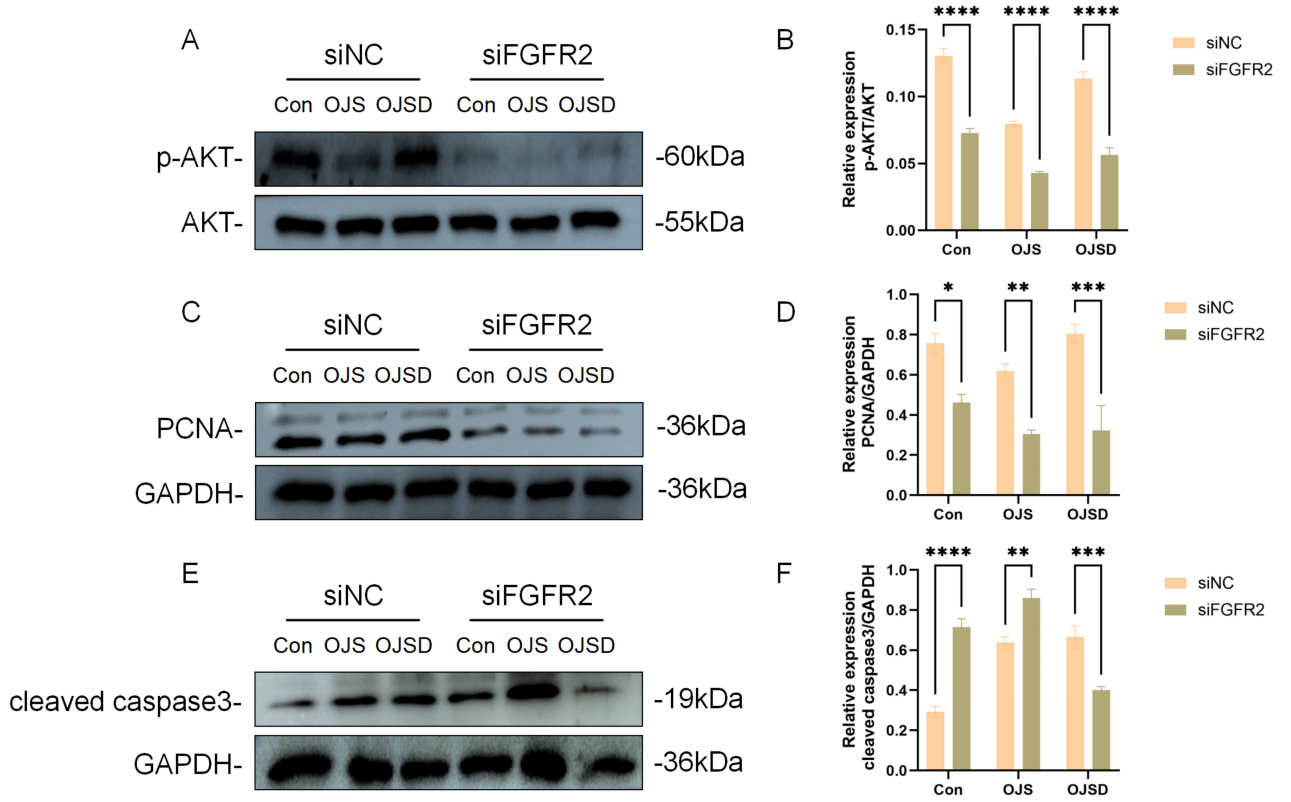

Fig. 8. FGFR2 knockdown suppresses AKT phosphorylation, alters PCNA expression, and modulates cleaved caspase-3 levels in BRL-3A cells under different serum conditions. (A) Representative Western blots of p-AKT and total AKT in siNC- and siFGFR2-transfected cells cultured under Con, OJS, and OJSD conditions. (B) Densitometric quantification of p-AKT normalized to total AKT. FGFR2 knockdown reduced p-AKT by approximately 50% in all three serum conditions compared with siNC controls (all $p < 0.01$). (C) Representative blots of PCNA and GAPDH. (D) Quantification of PCNA/GAPDH ratio. In siNC cells, PCNA decreased in OJS vs. Con ($p < 0.05$) and partially recovered in OJSD; FGFR2 knockdown further reduced PCNA, with the most pronounced decrease in OJSD ($p < 0.01$ vs. siNC-OJSD), and no significant difference between OJS and OJSD in siFGFR2 cells. (E) Representative blots of cleaved caspase-3 and GAPDH. (F) Quantification of cleaved caspase-3/GAPDH ratio. In siNC cells, OJS increased cleaved caspase-3 vs. Con ($p < 0.05$), but OJS and OJSD were not significantly different; siFGFR2 cells showed generally higher levels, yet in OJSD, siFGFR2 cells had lower cleaved caspase-3 than siNC-OJSD ($p < 0.05$). Data are mean ± SD (n = 3 independent experiments). Statistical significance is indicated as follows: *, $p < 0.05$; **, $p < 0.01$; ***, $p < 0.001$; ****, $p < 0.0001$. p-AKT, AKT phosphorylation; PCNA, proliferating cell nuclear antigen.

on the levels of p-ERK or p-STAT3 (all $p > 0.05$). These findings suggest that, within our experimental framework, FGFR2 knockdown does not influence the activation of ERK or STAT3, and that the cholestatic microenvironment alone does not markedly modulate these pathways in BRL-3A hepatocytes. Consequently, the functional effects of FGFR2 on cell proliferation and apoptosis are predominantly mediated via the PI3K/AKT pathway.

4. Discussion

OJ is a common clinical condition resulting from impaired bile excretion due to biliary obstruction, which subsequently induces a series of pathophysiological changes in the liver and systemic circulation [35]. As the central organ of bile metabolism, the liver is susceptible to multiple pathophysiological alterations due to cholestasis during the progression of OJ, primarily including hepatocyte injury, disruption of hepatic lobular architecture, inflammatory cell infiltration, and fibrous tissue proliferation. The liver repair process following R-OJ directly influences patient prognosis [36,37]. Therefore, clarifying the core regulatory mechanisms underlying liver injury and repair in OJ and identifying key regulatory targets are of significant importance for optimizing clinical treatment strategies. The OJ model is a classic tool for studying liver injury and repair. In this study, serum liver function indicators (ALT, AST, TBIL, DBIL) in the OJ group were significantly elevated compared with the Sham group, accompanied by severe destruction of hepatic tissue architecture. In contrast, both hepatic structure and serum indicators in the R-OJ group were sig-

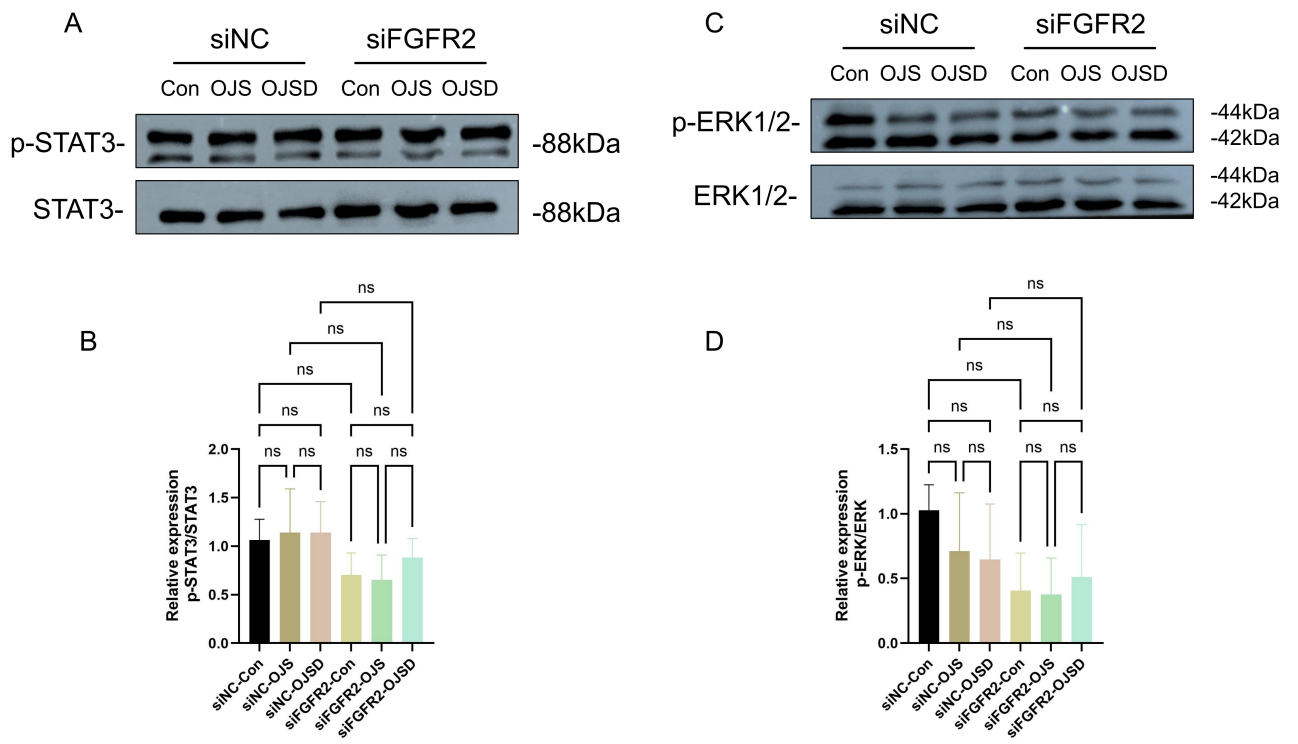

Fig. 9. Effect of FGFR2 knockdown on ERK and STAT3 phosphorylation. (A,C) Representative Western blots of p-STAT3, total STAT3, p-ERK and total ERK in siNC- and siFGFR2-transfected BRL-3A cells under Con, OJS, and OJSD conditions. (B,D) Densitometric quantification of p-STAT3/STAT3 and p-ERK/ERK ratios. Data are mean ± SD (n = 3 independent experiments). Two-way ANOVA revealed no significant differences between siNC and siFGFR2 groups, nor among the three serum conditions (all $p > 0.05$). ns, not significant. p-STAT3, STAT3 phosphorylation; p-ERK, ERK phosphorylation; ANOVA, Analysis of Variance.

nificantly improved relative to the OJ group. These results confirm that although OJ causes substantial structural and functional liver damage, the liver retains the capacity for reversible recovery following relief of obstruction. Ozozan et al. [12] similarly observed in a rat OJ model that after biliary obstruction relief, hepatic mitochondrial number increased alongside lipid metabolism remodeling, suggesting the initiation of liver regeneration . Through bioinformatics analysis, animal and cellular experiments, this study identified FGFR2 as a key regulatory molecule and provided evidence suggesting that FGFR2 is associated with pro-proliferative and pro-survival effects, potentially through the PI3K/AKT signaling axis, rather than through the ERK or STAT3 pathways. By integrating an *in vivo* obstruction–recanalization model with an *in vitro* staged serum model, this work provides a systematic framework for dissecting the molecular dynamics of cholestatic liver injury and repair. FGFR2 was found to be closely related to cell cycle regulation and PI3K/AKT signaling, and may contribute to promoting proliferation and inhibiting apoptosis during cholestatic liver repair.

This study achieved synchronous integration between an *in vivo* dynamic obstruction–recanalization model and an *in vitro* staged cell model that simulates the pathological microenvironment using disease serum, encompassing both injury and repair phases. Since tissue RNA-seq inherently contains mixed signals from all hepatic cell types, it is challenging to accurately attribute transcriptional changes to specific cell populations. By employing purified BRL-3A hepatocytes for RNA-seq analysis, we ensured that the observed FGFR2 expression dynamics are specifically attributable to hepatocytes, the principal functional cells of the liver. Through integrated bioinformatic analysis, including dynamic temporal differential expression, intersection with “injury” and “repair” gene sets, and PPI network construction, we identified FGFR2 as the core regulatory gene among 20 candidates. KEGG and GO enrichment analyses revealed that the MAPK signaling pathway, PI3K-AKT pathway, and processes related to angiogenesis and wound healing were closely associated with the injury and repair phenotypes [38,39,40]. As a cell surface receptor tyrosine kinase, FGFR2 transduces extracellular growth signals into intracellular instructions regulating cell proliferation, differentiation, and survival via activation of the MAPK cascade (RAS-RAF-MEK-ERK) and the PI3K-AKT pathway [41,42,43].

This study demonstrate that FGFR2 exhibits a dynamic expression pattern characterized by downregulation

during injury and upregulation during repair in the OJ model, both *in vivo* and *in vitro*. Previous studies have established that FGFR signaling is crucial for hepatocyte proliferation and liver regeneration. Padrissa-Altés et al. [17] showed that hepatocyte-specific disruption of FGFR signaling delays liver regeneration and leads to liver failure after partial hepatectomy. Zhang et al. [44] further demonstrated that miR-218-5p in liver-derived extracellular vesicles impairs hepatic regeneration by inhibiting FGFR2 signaling in patients with hepatitis B virus-related acute-on-chronic liver failure. Our observation of FGFR2 downregulation during OJ is consistent with these findings and suggests that impaired FGFR2 expression may contribute to the diminished regenerative capacity observed during cholestatic injury. Critically, the present study extends beyond expression-level correlation to establish a functional role for FGFR2 in OJ-related hepatocyte responses. Through siRNA-mediated knockdown of FGFR2 in BRL-3A cells, we demonstrated that FGFR2 loss significantly reduced AKT phosphorylation (p-AKT) by approximately 50% across all serum conditions (Con, OJS, and OJSD), confirming that FGFR2 is a major upstream activator of the PI3K/AKT pathway in hepatocytes. Furthermore, FGFR2 knockdown significantly decreased the expression of PCNA, a marker of cell proliferation, and altered the levels of cleaved caspase-3, a key executor of apoptosis. Notably, the recovery of PCNA expression observed in the OJSD repair phase was completely abolished in FGFR2-depleted cells, indicating that FGFR2 is not merely a passive marker of hepatocyte recovery but is functionally associated with the proliferative response during repair. Collectively, these loss-of-function experiments suggest that FGFR2 contributes to the regulation of hepatocyte proliferation and survival in the context of cholestatic injury and repair.

The regulatory role of FGFR2 in OJ appears to be mediated through the PI3K-AKT signaling axis. The substantial reduction in p-AKT upon FGFR2 knockdown aligns with previous reports that FGFR2 activates the PI3K-AKT pathway in hepatocellular carcinoma and colorectal cancer cells [45], and that SNORD126 promotes tumor growth through FGFR2-mediated AKT activation [18]. In the context of OJ, downregulation of FGFR2 during the injury phase likely suppresses pro-survival and pro-proliferative AKT signaling, contributing to hepatocyte growth arrest and increased apoptosis. Conversely, upregulation of FGFR2 during the repair phase restores AKT activity, thereby promoting hepatocyte regeneration and facilitating structural and functional recovery. As shown in Fig. 10, we mapped the relevant mechanism of FGFR2. In addition to the PI3K-AKT pathway, our RNA-seq data also identified the MAPK pathway as significantly enriched, and previous studies have demonstrated that FGFR2 can activate both cascades [18,41,43]. Future studies employing selective pathway inhibitors will be required to dissect the relative contributions of AKT versus ERK signaling to FGFR2-mediated repair. Beyond its direct effects on hepatocytes, FGFR2 may also influence the behavior of non-parenchymal cells in the liver microenvironment. Previous work has shown that FGFR2 inhibition attenuates hepatic stellate cell (HSC) activation and reduces liver fibrosis in preclinical models [46]. This raises the intriguing possibility that the dynamic regulation of FGFR2 during OJ and R-OJ could coordinately modulate both hepatocyte regeneration and fibrogenic responses. Further investigation using co-culture systems or hepatocyte-specific FGFR2 knockout models will be necessary to delineate the cell type-specific contributions of FGFR2 in cholestatic liver disease.

The findings of this study have potential translational implications. FGFR2 is already a clinically validated therapeutic target in oncology, with FGFR inhibitors such as futibatinib demonstrating efficacy in patients with FGFR2-rearranged intrahepatic cholangiocarcinoma [47]. Our data suggest that modulating FGFR2 activity could also be explored as a strategy to enhance liver repair following biliary decompression. For instance, transient pharmacological activation of FGFR2 during the early repair phase might accelerate hepatocyte regeneration and improve recovery in patients with severe OJ-induced liver injury. Conversely, in settings of prolonged biliary obstruction where fibrosis predominates, FGFR2 inhibition might help limit HSC activation and collagen deposition. However, given the dual roles of FGFR2 in both regeneration and fibrosis, careful timing and cell type-specific targeting would be essential to maximize therapeutic benefit while minimizing adverse effects.

Several limitations of this study should be acknowledged. First, while siRNA-mediated knockdown has established the functional requirement for FGFR2 in hepatocyte proliferation and survival, gain-of-function experiments (e.g., FGFR2 overexpression) were not performed to determine whether enhancing FGFR2 activity is sufficient to accelerate repair. Second, the *in vitro* model focused exclusively on hepatocytes and did not capture potential crosstalk with HSCs, cholangiocytes, or Kupffer cells, which are known to participate in OJ pathophysiology. Third, although we validated FGFR2 expression dynamics in rat models and cell lines, the relevance of these findings to human cholestatic liver diseases requires confirmation in clinical specimens. Fourth, the functional conclusions drawn from this study are mainly based on *in vitro* siRNA-mediated knockdown experiments conducted in the BRL-3A hepatocyte cell line. Although these loss-of-function data indicate that depletion of FGFR2 impairs AKT signaling, decreases proliferation markers, and modifies apoptosis, the current findings suggest an association between FGFR2 and hepatocyte repair rather than conclusively establishing a definitive causal relationship. To determine the causal role of FGFR2 in liver repair following obstructive jaundice, *in vivo* gain- and loss-of-function studies uti-

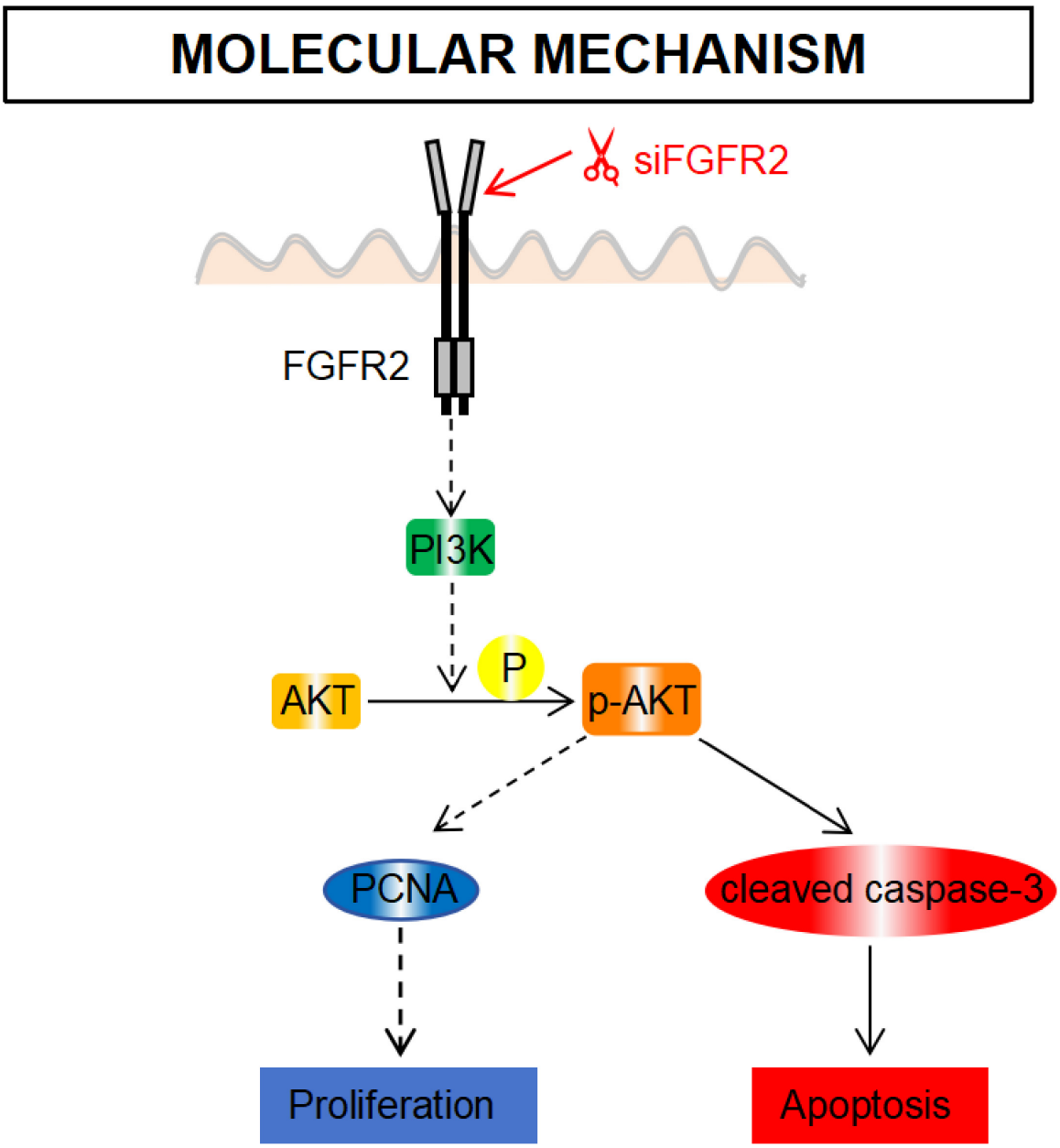

Fig. 10. The molecular mechanism elucidates the activation of the PI3K/AKT signaling pathway mediated by FGFR2. Knockdown of FGFR2 using siRNA reduces AKT phosphorylation (p-AKT), leads to a decrease in the expression of the proliferation marker PCNA, and alters the levels of caspase-3 cleaved by key apoptotic execution factors. These findings suggest that FGFR2 may represent an important upstream regulator of hepatocyte proliferation and survival during cholestatic injury and repair processes. PI3K, phosphoinositide 3-kinase.

lizing hepatocyte-specific genetic models will be essential. Future studies will address these limitations by employing hepatocyte-specific FGFR2 transgenic mice, establishing co-culture systems to investigate intercellular communication, and analyzing FGFR2 expression and activation status in liver biopsies from patients with biliary atresia, primary sclerosing cholangitis, or malignant biliary obstruction.

5. Conclusions

Our research has confirmed for the first time that FGFR2 exhibits a dynamic expression pattern of "down-regulation during the injury phase and upregulation during the repair phase" in the process of OJ-induced liver injury and repair. Therefore, FGFR2 may act as a key regulatory factor involved in the core process of OJ-related liver in-

jury repair. This finding provides a potential target for further understanding the molecular pathogenesis of OJ and developing novel therapeutic strategies. Furthermore, loss-of-function studies suggest that FGFR2 may be involved in regulating hepatocyte proliferation and apoptosis, potentially via AKT signaling, which implies that FGFR2 could represent a potential therapeutic target for obstructive jaundice.

6. Future Perspectives

Based on the findings of this study, future research can proceed in the following key directions. Firstly, while our *in vitro* siRNA knockdown experiments have confirmed the causal role of FGFR2 in hepatocytes' response to cholestatic injury and repair, future studies should still employ hepatocyte-specific FGFR2 knockout mice to validate the authenticity of these findings within the complex liver microenvironment using OJ and recanalization models. Secondly, given that the pathophysiology of obstructive jaundice involves intricate interactions among various cell types, including hepatocytes, hepatic stellate cells, cholangiocytes, and Kupffer cells, future research should utilize co-culture systems or single-cell RNA sequencing technology to elucidate how FGFR2-positive hepatocytes communicate with adjacent non-parenchymal cells to jointly regulate fibrosis and regeneration processes. Thirdly, to enhance the translational relevance of the study, it is imperative to verify the expression and activation status of FGFR2 in human cholestatic liver disease samples, such as those from patients with biliary atresia, primary sclerosing cholangitis, or malignant biliary obstruction. Fourthly, the upstream mechanisms regulating the dynamic expression of FGFR2 during injury and repair remain unclear; future studies should investigate epigenetic modifications, transcription factors, and non-coding RNAs (such as miRNAs and lncRNAs) that may modulate FGFR2 transcription or mRNA stability. Fifthly, based on the interaction between FGFR2 and TGF-β signaling suggested by this study and previous reports [46], research utilizing a hepatocyte-hepatic stellate cell co-culture model should be conducted to elucidate the role of FGFR2 in the onset and resolution of fibrosis.Ultimately, assessing the therapeutic efficacy of FGFR2 modulators in suitable animal models, for instance, employing selective agonists to facilitate regeneration during the repair phase or utilizing specific inhibitors to avert excessive fibrosis during the injury phase, can provide a cornerstone for the development of innovative therapeutic approaches for patients afflicted with obstructive jaundice.

Availability of Data and Materials

The datasets used and analyzed during the current study are available from the corresponding author upon reasonable request.

Author Contributions

JY, BC, JH: concept and design of this study. WC, JL, HX: conducted experiments and analyzed data. WC, JL, JY, JH: conducted experiments and analyzed data. WC, XL, PL, GC, DL: interpreted data. WC, JL: drafted the manuscript. JY, BC, JH: reviewed data and proofread manuscripts. All authors read and approved the final manuscript. All authors have participated sufficiently in the work and agreed to be accountable for all aspects of the work. All authors contributed to editorial changes in the manuscript.

Ethics Approval and Consent to Participate

All animal experiments were approved by the Biomedical Research Ethics Committee of Anhui University of Science and Technology (approval No. LZ2023-002), and all experiments were conducted in accordance with local and national guidelines and regulations. The study was carried out in accordance with the ARRIVE guidelines.

Acknowledgment

The authors thank the Anhui Provincial Key Laboratory of Occupational Health, Anhui No. 2 Provincial People's Hospital for support. The authors would like to thank Dr. Fang Tong for her contribution to project administration and ethical oversight of this study.

Funding

This work was financially supported by the University Research Project of Anhui Province (KJ2020A0854), the Scientific Research Project of Anhui Provincial Healthcare Commission (2024AH050542, AHWJ2023A20214), the Scientific Research Project of Anhui Medical University (2023XKJ116).

Conflicts of Interest

The authors declare no conflicts of interest.

Supplementary Material

Supplementary material associated with this article can be found, in the online version, at https://doi.org/10.31083/FBL49296.

References

[1] Pavlidis ET, Pavlidis TE. Pathophysiological consequences of obstructive jaundice and perioperative management. Hepatobiliary & Pancreatic Diseases International : HBPD INT. 2018; 17: 17–21. https://doi.org/10.1016/j.hbpd.2018.01.008

[2] Alshoabi SA, Binnuhaid AA, Muslem HF, Hamid AM, Alhazmi FH, Alrehily FA, et al. Demographic Profiles, Etiological Spectrum, and Anatomical Locations of the Post-Hepatic Obstructive Jaundice in Adult Population in Hadhramout Region in Yemen. Diseases (Basel, Switzerland). 2024; 12: 333. https://doi.org/10.3390/diseases12120333

[3] Kaomba L, Ng'ombe J, Mulwafu W. Clinicopathological features and management of obstructive jaundice at Queen Elizabeth Central Hospital, Malawi. A retrospective cohort analysis. Surgery Open Science. 2024; 20: 14–19. https://doi.org/10.1016/j.sopen.2024.05.004
[4] Kwak JY, Jeon H, Kim SJ, Han JH, Cha RR, Lee SS. Etiology and Outcomes of Patients with Extreme Hyperbilirubinemia in Korea: A Retrospective Cohort Study. The Korean Journal of Gastroenterology = Taehan Sohwagi Hakhoe Chi. 2024; 84: 9–16. https://doi.org/10.4166/kjg.2024.038
[5] Kullak-Ublick GA, Meier PJ. Mechanisms of cholestasis. Clinics in Liver Disease. 2000; 4: 357–385. https://doi.org/10.1016/s1089-3261(05)70114-8
[6] Pellicoro A, Ramachandran P, Iredale JP, Fallowfield JA. Liver fibrosis and repair: immune regulation of wound healing in a solid organ. Nature Reviews. Immunology. 2014; 14: 181–194. https://doi.org/10.1038/nri3623
[7] Campana L, Esser H, Huch M, Forbes S. Liver regeneration and inflammation: from fundamental science to clinical applications. Nature Reviews. Molecular Cell Biology. 2021; 22: 608–624. https://doi.org/10.1038/s41580-021-00373-7
[8] Seo E, Kang H, Choi H, Choi W, Jun HS. Reactive oxygen species-induced changes in glucose and lipid metabolism contribute to the accumulation of cholesterol in the liver during aging. Aging Cell. 2019; 18: e12895. https://doi.org/10.1111/acel.12895
[9] Liu J, Hu J, Xu H, Yan L, Yao J, Cao B. Role of VDAC1 in hepatocyte apoptosis during acute liver injury in rats induced by obstructive jaundice. Iranian Journal of Basic Medical Sciences. 2025; 28: 87–97. https://doi.org/10.22038/ijbms.2024.78454.16962
[10] Ren HM, Yang LQ, Liu ZQ, Chen CY, Cheung CW, Tao KM, et al. In vivo and ex vivo effects of propofol on myocardial performance in rats with obstructive jaundice. BMC Gastroenterology. 2011; 11: 144. https://doi.org/10.1186/1471-230X-11-144
[11] Acar S, Cetin R, Zihni I, Ozmen O, Sabuncuoglu MZ, Sozen I, et al. The effects of rose oil on liver damage in an experimental model of obstructive jaundice. Ulusal Travma Ve Acil Cerrahi Dergisi = Turkish Journal of Trauma & Emergency Surgery : TJTES. 2025; 31: 495–504. https://doi.org/10.14744/tjtes.2025.96613
[12] Ozozan OV, Dinc T, Vural V, Ozogul C, Ozmen MM, Coskun F. An electron microscopy study of liver and kidney damage in an experimental model of obstructive jaundice. Annali Italiani Di Chirurgia. 2020; 91: 122–130.
[13] Wang Q, Li ZX, Liu BW, He ZG, Liu C, Chen M, et al. Altered expression of differential gene and lncRNA in the lower thoracic spinal cord on different time courses of experimental obstructive jaundice model accompanied with altered peripheral nociception in rats. Oncotarget. 2017; 8: 106098–106112. https://doi.org/10.18632/oncotarget.22532
[14] Ramachandran P, Balamurali D, Peter JJ, Kumar MM, Safwan M, Vij M, et al. RNA-seq reveals outcome-specific gene expression of MMP7 and PCK1 in biliary atresia. Molecular Biology Reports. 2019; 46: 5123–5130. https://doi.org/10.1007/s11033-019-04969-3
[15] Tracey KJ, Cerami A. Tumor necrosis factor, other cytokines and disease. Annual Review of Cell Biology. 1993; 9: 317–343. https://doi.org/10.1146/annurev.cb.09.110193.001533
[16] Diehl AM. Cytokine regulation of liver injury and repair. Immunological Reviews. 2000; 174: 160–171. https://doi.org/10.1034/j.1600-0528.2002.017411.x
[17] Padrissa-Altés S, Bachofner M, Bogorad RL, Pohlmeier L, Rossolini T, Böhm F, et al. Control of hepatocyte proliferation and survival by Fgf receptors is essential for liver regeneration in mice. Gut. 2015; 64: 1444–1453. https://doi.org/10.1136/gutjnl-2014-307874
[18] Fang X, Yang D, Luo H, Wu S, Dong W, Xiao J, et al. SNORD126 promotes HCC and CRC cell growth by activating the PI3K-AKT pathway through FGFR2. Journal of Molecular Cell Biology. 2017; 9: 243–255. https://doi.org/10.1093/jmcb/mjw048
[19] Seitz T, Hellerbrand C. Role of fibroblast growth factor signalling in hepatic fibrosis. Liver International : Official Journal of the International Association for the Study of the Liver. 2021; 41: 1201–1215. https://doi.org/10.1111/liv.14863
[20] Hotta K, Kitamoto T, Kitamoto A, Ogawa Y, Honda Y, Kessoku T, et al. Identification of the genomic region under epigenetic regulation during non-alcoholic fatty liver disease progression. Hepatology Research : the Official Journal of the Japan Society of Hepatology. 2018; 48: E320–E334. https://doi.org/10.1111/hepr.12992
[21] Geervliet E, Terstappen LWMM, Bansal R. Hepatocyte survival and proliferation by fibroblast growth factor 7 attenuates liver inflammation, and fibrogenesis during acute liver injury via paracrine mechanisms. Biomedicine & Pharmacotherapy = Biomedecine & Pharmacotherapie. 2023; 167: 115612. https://doi.org/10.1016/j.biopha.2023.115612
[22] Jeong A, Lim Y, Kook T, Kwon DH, Cho YK, Ryu J, et al. Circular RNA circSMAD4 regulates cardiac fibrosis by targeting miR-671-5p and FGFR2 in cardiac fibroblasts. Molecular Therapy. Nucleic Acids. 2023; 34: 102071. https://doi.org/10.1016/j.omtn.2023.102071
[23] Zou Y, Yue P, Cao H, Wu L, Xu L, Liu Z, et al. A novel ameliorated rat model of reversible obstructive jaundice. Journal of Zhejiang University. Science. B. 2023; 24: 345–351. https://doi.org/10.1631/jzus.B2200421
[24] Sharma P. Value of Liver Function Tests in Cirrhosis. Journal of Clinical and Experimental Hepatology. 2022; 12: 948–964. https://doi.org/10.1016/j.jceh.2021.11.004
[25] Cardiff RD, Miller CH, Munn RJ. Manual hematoxylin and eosin staining of mouse tissue sections. Cold Spring Harbor Protocols. 2014; 2014: 655–658. https://doi.org/10.1101/pdb.prot073411
[26] Woolbright BL, Dorko K, Antoine DJ, Clarke JI, Gholami P, Li F, et al. Bile acid-induced necrosis in primary human hepatocytes and in patients with obstructive cholestasis. Toxicology and Applied Pharmacology. 2015; 283: 168–177. https://doi.org/10.1016/j.taap.2015.01.015
[27] Shen X, Zhang X, Li K, Huang G, Li X, Hou Y, et al. Combined bacterial translocation and cholestasis aggravates liver injury by activation pyroptosis in obstructive jaundice. Heliyon. 2024; 10: e35793. https://doi.org/10.1016/j.heliyon.2024.e35793
[28] Trovato FM, Zia R, Napoli S, Wolfer K, Huang X, Morgan PE, et al. Dysregulation of the Lysophosphatidylcholine/Autotaxin/Lysophosphatidic Acid Axis in Acute-on-Chronic Liver Failure Is Associated With Mortality and Systemic Inflammation by Lysophosphatidic Acid-Dependent Monocyte Activation. Hepatology (Baltimore, Md.). 2021; 74: 907–925. https://doi.org/10.1002/hep.31738
[29] de Carvalho TG, Pellenz FM, Laureano A, da Rocha Silla LM, Giugliani R, Baldo G, et al. A simple protocol for transfecting human mesenchymal stem cells. Biotechnology Letters. 2018; 40: 617–622. https://doi.org/10.1007/s10529-018-2505-8
[30] Love MI, Huber W, Anders S. Moderated estimation of fold change and dispersion for RNA-seq data with DESeq2. Genome Biology. 2014; 15: 550. https://doi.org/10.1186/s13059-014-0550-8
[31] Liu C, Yin Z, Feng T, Zhang M, Zhou Z, Zhou Y. An integrated network pharmacology and RNA-Seq approach for exploring the preventive effect of Lonicerae japonicae flos on LPS-induced acute lung injury. Journal of Ethnopharmacology. 2021;

264: 113364. https://doi.org/10.1016/j.jep.2020.113364
[32] Bustin SA, Ruijter JM, van den Hoff MJB, Kubista M, Pfaffl MW, Shipley GL, et al. MIQE 2.0: Revision of the Minimum Information for Publication of Quantitative Real-Time PCR Experiments Guidelines. Clinical Chemistry. 2025; 71: 634–651. https://doi.org/10.1093/clinchem/hvaf043
[33] Sule R, Rivera G, Gomes AV. Western blotting (immunoblotting): history, theory, uses, protocol and problems. BioTechniques. 2023; 75: 99–114. https://doi.org/10.2144/btn-2022-0034
[34] Mebratie DY, Dagnaw GG. Review of immunohistochemistry techniques: Applications, current status, and future perspectives. Seminars in Diagnostic Pathology. 2024; 41: 154–160. https://doi.org/10.1053/j.semdp.2024.05.001
[35] Liu JJ, Sun YM, Xu Y, Mei HW, Guo W, Li ZL. Pathophysiological consequences and treatment strategy of obstructive jaundice. World Journal of Gastrointestinal Surgery. 2023; 15: 1262–1276. https://doi.org/10.4240/wjgs.v15.i7.1262
[36] Santiago P, Scheinberg AR, Levy C. Cholestatic liver diseases: new targets, new therapies. Therapeutic Advances in Gastroenterology. 2018; 11: 1756284818787400. https://doi.org/10.1177/1756284818787400
[37] Li J, Zhu X, Zhang M, Zhang Y, Ye S, Leng Y, et al. Limb expression 1-like (LIX1L) protein promotes cholestatic liver injury by regulating bile acid metabolism. Journal of Hepatology. 2021; 75: 400–413. https://doi.org/10.1016/j.jhep.2021.02.035
[38] Di HT, Wu XZ, Wang HQ, Chen M, Kong EL, Yu WF, et al. Involvement of the p38 MAPK-pHsp27 pathway in vascular hyporeactivity induced by obstructive jaundice in rats. Biomedicine & Pharmacotherapy = Biomedecine & Pharmacotherapie. 2020; 121: 109304. https://doi.org/10.1016/j.biopha.2019.109304
[39] Lin Y, Gil CH, Banno K, Yokoyama M, Wingo M, Go E, et al. ABCG2-Expressing Clonal Repopulating Endothelial Cells Serve to Form and Maintain Blood Vessels. Circulation. 2024; 150: 451–465. https://doi.org/10.1161/CIRCULATIONAHA.122.061833
[40] Li Z, Solomonidis EG, Meloni M, Taylor RS, Duffin R, Dobie R, et al. Single-cell transcriptome analyses reveal novel targets modulating cardiac neovascularization by resident endothelial cells following myocardial infarction. European Heart Journal. 2019; 40: 2507–2520. https://doi.org/10.1093/eurheartj/ehz305
[41] Meric-Bernstam F, Bahleda R, Hierro C, Sanson M, Bridgewater J, Arkenau HT, et al. Futibatinib, an Irreversible FGFR1-4 Inhibitor, in Patients with Advanced Solid Tumors Harboring FGF/FGFR Aberrations: A Phase I Dose-Expansion Study. Cancer Discovery. 2022; 12: 402–415. https://doi.org/10.1158/2159-8290.CD-21-0697
[42] Lau WM, Teng E, Huang KK, Tan JW, Das K, Zang Z, et al. Acquired Resistance to FGFR Inhibitor in Diffuse-Type Gastric Cancer through an AKT-Independent PKC-Mediated Phosphorylation of GSK3β. Molecular Cancer Therapeutics. 2018; 17: 232–242. https://doi.org/10.1158/1535-7163.MCT-17-0367
[43] DiPeri TP, Zhao M, Evans KW, Varadarajan K, Moss T, Scott S, et al. Convergent MAPK pathway alterations mediate acquired resistance to FGFR inhibitors in FGFR2 fusion-positive cholangiocarcinoma. Journal of Hepatology. 2024; 80: 322–334. https://doi.org/10.1016/j.jhep.2023.10.041
[44] Zhang S, Yu J, Rao K, Cao J, Ma L, Yu Y, et al. Liver-derived extracellular vesicles from patients with hepatitis B virus-related acute-on-chronic liver failure impair hepatic regeneration by inhibiting on FGFR2 signaling via miR-218-5p. Hepatology International. 2023; 17: 833–849. https://doi.org/10.1007/s12072-023-10513-0
[45] Tian C, Li Y, Wang L, Si J, Zheng Y, Kang J, et al. Blockade of FGF2/FGFR2 partially overcomes bone marrow mesenchymal stromal cells mediated progression of T-cell acute lymphoblastic leukaemia. Cell Death & Disease. 2022; 13: 922. https://doi.org/10.1038/s41419-022-05377-5
[46] Meng Q, Luo L, Lei M, Chen Z, Sun Y, Chen X, et al. Inhibition of FGFR2 Signaling by Cynaroside Attenuates Liver Fibrosis. Pharmaceuticals (Basel, Switzerland). 2023; 16: 548. https://doi.org/10.3390/ph16040548
[47] Goyal L, Meric-Bernstam F, Hollebecque A, Valle JW, Morizane C, Karasic TB, et al. Futibatinib for FGFR2-Rearranged Intrahepatic Cholangiocarcinoma. The New England Journal of Medicine. 2023; 388: 228–239. https://doi.org/10.1056/NEJMoa2206834